# Targeting FUS with High-Fidelity Cas13d Nucleases

*Mayuri Singh[1], Neil A. Shneider[2], and Thomas Gaj[1]*

[1]*Department of Bioengineering, University of Illinois Urbana-Champaign, Urbana, IL*

[2]*Department of Neurology, Center for Motor Neuron Biology and Disease, Columbia University, New York, NY, USA*

GAJ LAB

## Research overview

Over 50 mutations in the RNA/DNA-binding protein FUS have been identified in ALS patients, many of which are believed to exert a toxic gain-of-function effect. We determined whether RfxCas13d, an RNA-targeting CRISPR nuclease compatible with a single-AAV delivery, can be used to silence FUS. To minimize off-target effects, we employed high fidelity (HF) variants N2V7 and N2V8, which reduce collateral degradation of non-target transcripts. We designed 40 crRNAs targeting the FUS coding sequence and evaluated their targeting in HEK293T cells, with top candidate achieving >80% transcript reduction and >90% protein reduction relative to non-targeting controls. Transcriptome-wide effects were analyzed via RNA-seq. Top-performing variants will be delivered via AAV9 to FUS-ALS rodent models to evaluate suppression of WT and mutant FUS RNA and protein in vivo.

## Targeting FUS with HF-RfxCas13d

We sought to determine if high-fidelity variants of RfxCas13d, namely N2V7 and N2V8, could reduce FUS expression in HEK293T cells

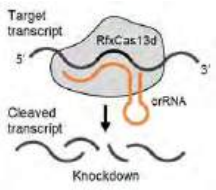


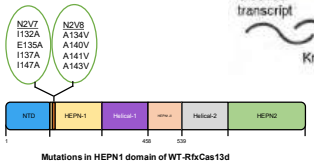


Using the Cas13d Design Resource, we identified 40 crRNAs targeting the FUS gene. These variants were cloned alongside N2V7-RfxCas13d and N2V8-RfxCas13d.

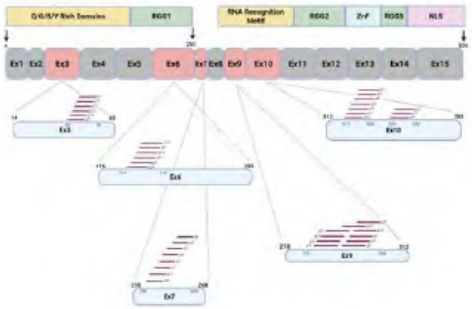


The top 40 FUS-targeting crRNAs are clustered around exon 3, exon 6, exon 7, exon 9, and exon 10.

## Reducing FUS mRNA in vitro with HF-RfxCas13d

Using qPCR, we measured FUS mRNA in HEK293T cells transfected with each variant.

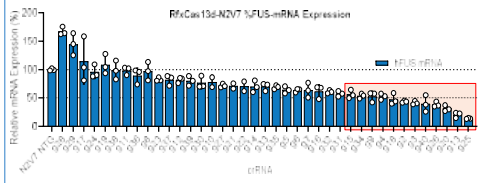


- For N2V7-RfxCas13d, we observed a >50% decrease in FUS mRNA with 12 crRNAs, with the top-performing crRNA showing a >85% reduction.

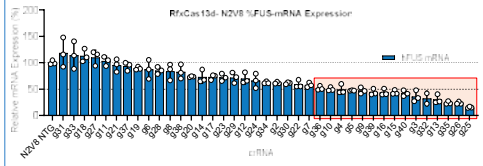


- For N2V8-RfxCas13d, we observed a >50% decrease in FUS mRNA reduction for 15 crRNAs, with the best performing crRNA showing >80% reduction

## Reducing FUS protein in vitro with HF-RfxCas13d

The top 8 crRNAs for both N2V7-RfxCas13d and N2V8-RfxCas13d were analyzed in HEK293T cells for their ability to lower FUS protein

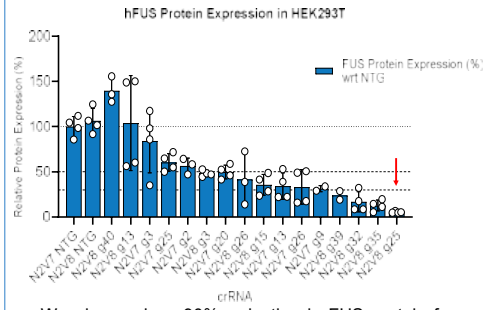


- We observed a ~90% reduction in FUS protein for the most effective variant.

## Collateral cleavage of FUS-targeting HF-RfxCas13d

To assess the collateral effects of HF-RfxCas13d, we transfected each variant with a bystander reporter, mCherry, and measured change in fluorescence intensity.

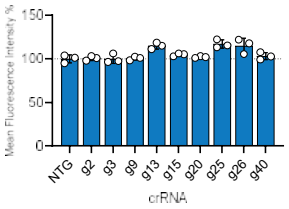


- N2V7-RfxCas13d-crRNAs showed negligible collateral effects

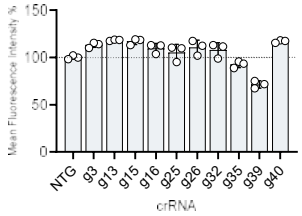


- All but two N2V8-RfxCas13d-crRNAs showed negligible collateral effects

## Differentially Expressed Genes (DEGs) from Targeting FUS in HEK293T cells

Using RNA-sequencing, we did transcriptomic profiling in HEK293T cells to characterize differential gene expression patterns resulting from targeted perturbation of the FUS RNA-binding protein.

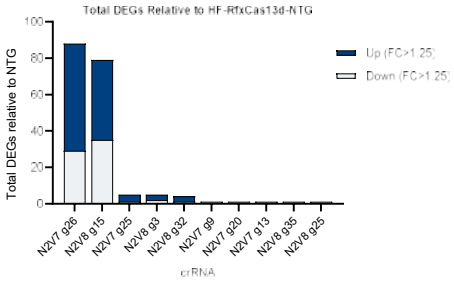


- The most specific crRNAs induced <5 DEGs, with FUS observed as the most affected transcript.

## Validating FUS mRNA Knockdown in SH-SY5Y

Lead crRNAs identified were subsequently validated in SH-SY5Y neuroblastoma cells to confirm on-target activity and assess efficacy in a neurologically relevant cellular model

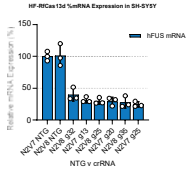


- Top performing HF-RfxCas13d crRNAs showed ~70% reduction in FUS mRNA in SH-SY5Y cells

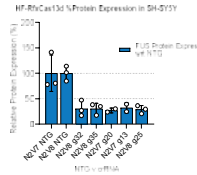


- Top performing HF-RfxCas13d crRNAs showed ~70% reduction in FUS protein levels in SH-SY5Y cells

## Conclusions

- HF-RfxCas13d can reduce FUS mRNA and protein in vitro.
- HF-RfxCas13d variants (N2V7 and N2V8) showed no detectable collateral RNA cleavage
- Based on RNA-seq, the most specific HF-RfxCas13d variants induced no detectable DEGs beyond FUS.

## Future Direction

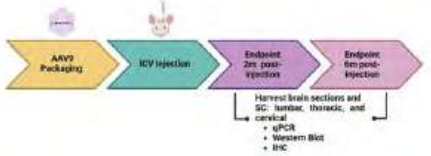


- The two leads crRNAs will be packaged in AAV9
- AAV9 vector will be injected via ICV-administration into FUS-ALS mice (N. Shneider lab).
- FUS RNA and protein levels will be quantified
- Transcriptome-wide specificity will be assessed with RNA-seq
- The ability for RfxCas13d to mediate trans-splicing to replace FUS exon 15 is also under active investigation.

## Acknowledgments

TARGET ALS

Target ALS, Novel Modalities Consortia (Grant No. NM-2025-C2-L1)

# Multi-Component Functional Profiling of Proteins in ALS: *A Novel Serum Biomarker Platform*

*Kirti Shila Sonkar, Vito Levi D'Ancona, Jade Cramp, Hannah Shilling, Ellie Giles,, Ghazaleh Sadri Vakili, Emanuele Buratti, Ian P. Thrippleton*

*Nemdx, Massachusetts, USA & Kent, UK*

*Collaborating institutions: Mass General Brigham • NIH/NINDS • Johns Hopkins • Barrow Neurological Institute • University of Brescia • ICGEB • Massachusetts General Hospital • Brescia Hospital • TARGET ALS*

## BACKGROUND & RATIONALE

**Pathology hallmark**: Nuclear depletion, cytoplasmic mislocalization, hyper-phosphorylation, and aggregation into insoluble inclusions—found in > 96% of ALS cases.

- **GAP:** The Gap: ALS and related neurodegenerative diseases are defined by protein dysfunction (mislocalization, aggregation). Current blood biomarkers measure protein abundance (e.g., NFL concentration), not functional competence.
- **TDP-43 Pathology:** Present in >96% of ALS cases. Nuclear depletion and cytoplasmic aggregation impair its native RNA-binding function.
- **Objective:** To develop and validate a serum-based platform that quantifies the biochemical function of TDP-43 and extends modularly to other neurodegeneration markers (NFL, tau)

**Current Biomarker Limitations**

- Existing ALS biomarkers like neurofilament light chain (NfL) reflect axonal injury and neurodegeneration broadly, rather than ALS-specific TDP-43 pathology.
- TDP-43 shows weak correlation with NfL (r = 0.04–0.12), indicating complementary mechanistic information.

## METHODS

**Binding Technology:** Nemdx proprietary computationally-engineered RNA- to protein binder

Signal Generating Technology: hTR-FRET signal generation platform on standard plate readers

### Mechanistic Basis

TDP-43 binds UU-rich RNA motifs via tandem RRM domains. We engineered synthetic, nuclease-resistant RNA probes (2'-O-methyl modified) that bridge only in the presence of motif-competent TDP-43.

**Detection Physics:**
Homogeneous Time-Resolved FRET (hTR-FRET)

| Donor | Acceptor |
|---|---|
| Streptavidin-Terbium cryptate<br>τ ≈ 1.5-1.6 ms | Red-emitting fluorophore<br>Emission ≈ 665 nm |


### TDP-43 functional activity assay

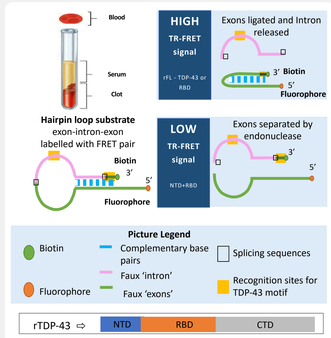


**Method Summary**

| Sample Volume | Assay Time |
|---|---|
| 5 µL | 60 min |
| **Sensitivity** | **Platform** |
| < pg/mL | hTR-FRET |

### NFL/Tau quantification assay

Signal read when both RNA probes bind to Target

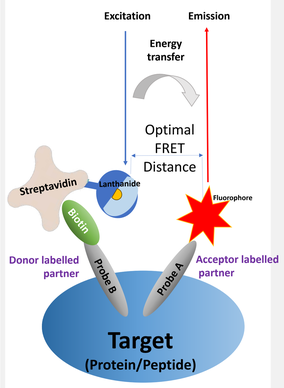


## RESULTS

### Assay Characteristics

**TDP-43 functional activity**
5µl serum | CVs < 5%

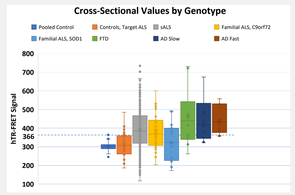


**NfL quantification**
0.5-500 pg/ml | 5µl serum | CVs < 5%

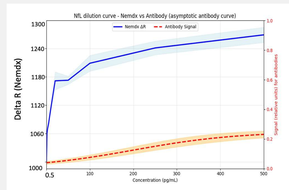


**Tau quantification**
0.02-25 pg/ml | 5µl serum | CVs < 5%

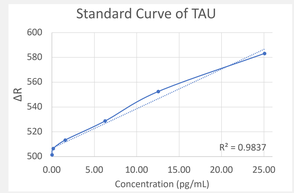


TDP-43 functional activity assay results:

- **Sporadic vs. Familial ALS:** Sporadic ALS shows highest activity (392 a.u.), with C9orf72 carriers slightly lower (382 a.u.), suggesting genotype-specific RNA dysregulation patterns.
- **SOD1-ALS:** Unexpected Finding SOD1-ALS shows elevated TDP-43 activity (323 a.u.) despite traditional exclusion from TDP-43 proteinopathies, supporting emerging mechanistic links.
- **Comparator Diseases:** FTD and AD show even higher values than ALS, indicating potential disease-specific patterns requiring validation in larger cohorts.

NfL quantification comparative results:

| Sample ID | Study | A Data | B Data |
|---|---|---|---|
| 146 | Bio-02 | 67 | 63 |
| 83 | Bio-02 | 35 | 28 |
| 87 | Bio-02 | 21 | 29 |
| 183 | Bio-02 | 20 | 38 |
| 55 | Bio-02 | 25 | 12 |
| 79 | Bio-02 | 12 | 6 |
| 206 | Bio-02 | 12 | 2 |

A Data from Huang et al., Ann. Clin. Transl. Neurol. (2020)

B Data generated in-house at Nemdx

### Multi Component Analysis

**ALS vs Tau-FTD vs AD subtypes**

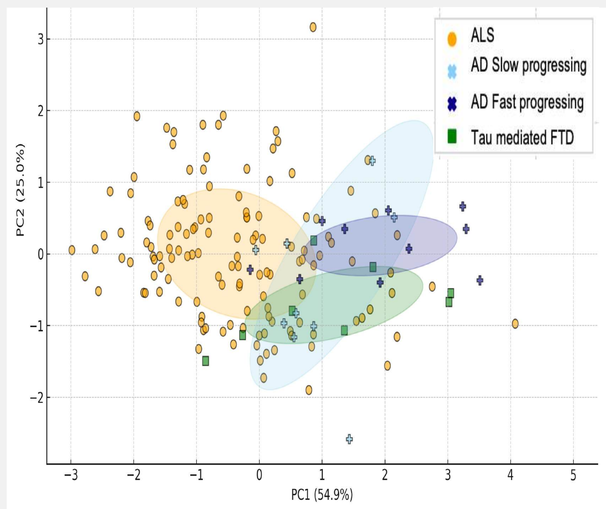


**DIAGNOSTIC DISTINCTION**

1. PC1 separates conditions by total pathological burden (TDP-43 Modulation) & tau); PC2 refines distinction based on NfL-driven axonal injury
2. ALS samples cluster separately toward the bottom left, supporting diagnostic distinction
3. Tau-Mediated FTD overlaps more with both AD variants, but remains visually distinct from ALS

## CONCLUSIONS & SCIENTIFIC IMPACT

This functional proteomic tool bridges molecular pathology and clinical application, enabling *in vivo* drug efficacy assessment for TDP-43-directed ALS therapies.

**Paradigm Shift in Biomarker Development**
The hTR-FRET TDP-43 functional assay represents a fundamental shift from measuring static protein presence to quantifying dynamic biochemical function—the first direct biofluid evidence of TDP-43 functional state in human disease.

- **Diagnostic Impact**: AUC = 0.79 with 95% specificity enables confident ALS discrimination from healthy controls
- **Therapeutic Impact:** Direct functional measurement enables target engagement and drug efficacy assessment

**Key Scientific Contributions**

1. First functional biomarker: Direct measurement of TDP-43 RNA-binding activity in serum using hTR-FRET technology
2. Large-scale validation: 1,080 samples from 8 international cohorts demonstrating robust diagnostic performance
3. Genotype insights: SOD1-ALS elevation challenges traditional TDP-43 proteinopathy boundaries
4. Progression monitoring: Longitudinal correlation with clinical decline supports pharmacodynamic utility
5. Interpretable results at low concentrations: Where antibody assays approach the noise floor, Nemdx maintains a linear interpretable response at low concentrations.

**Clinical Translation Pathway**

1. **Diagnostic Confirmation**: 95% specificity threshold for ALS diagnosis
2. **Trial Stratification**: Genotype-specific patient enrollment
3. **Drug Development**: Pharmacodynamic endpoint for TDP-43 therapies

## REFERENCES

- Bhardwaj, A., et al. (2013). "Characterizing TDP-43 interaction with its RNA targets." Nucleic acids research 41(9): 5062-5074.
- Buratti, E. and F. E. Baralle (2001). "Characterization and functional implications of the RNA binding properties of nuclear factor TDP-43, a novel splicing regulator of CFTR exon 9." Journal of Biological Chemistry 276(39): 36337-36343.
- Huang, F., et al. (2020). "Longitudinal biomarkers in amyotrophic lateral sclerosis." Annals of clinical and translational neurology 7(7): 1103-1116.
- Luthi-Carter, R., et al. (2024). "Location and function of TDP-43 in platelets, alterations in neurodegenerative diseases and arising considerations for current plasma biobank protocols." Scientific reports 14(1): 21837.
- Neumann, M., et al. (2006). "Ubiquitinated TDP-43 in frontotemporal lobar degeneration and amyotrophic lateral sclerosis." Science 314(5796): 130-133.

**Acknowledgement: ALS Funding A Cure**

# DYSFUNCTIONAL OLIGODENDROCYTES IN AMYOTROPHIC LATERAL SCLEROSIS: TARGETS OF THERAPY AND SOURCES OF NEW POTENTIAL BIOMARKERS


**Marta Fumagalli[1], Stefano Raffaele[1], Tiziana Bonifacino[2], Nhung Nguyen[2], Elena M. Chinosi[1], Alessia Becchetti[1], Claudia Verderio[3], Marina Camera[1], Maria P. Abbracchio[1]**

*[1]Department of Pharmaceutical Sciences, section "Pharmacology and Bioscience", Università degli Studi di Milano, 20133 Milan, Italy*
*[2]Department of Pharmacy, section "Pharmacology and Toxicology", Università degli Studi di Genova, Genoa, Italy*
*[3]CNR Institute of Neuroscience, Vedano al Lambro, Monza, Italy*


## BACKGROUND

1. **Oligodendrocytes (OLs) myelinate axons and provide trophic and metabolic support to motor neurons (MNs) in the central nervous system (CNS). In ALS, early loss of mature oligodendrocytes and accumulation of dysfunctional oligodendrocyte precursors cells (OPCs) lead to impaired myelination and reduced neuronal support, contributing to motor neuron degeneration. Promoting OPC maturation may offer therapeutic potential.**

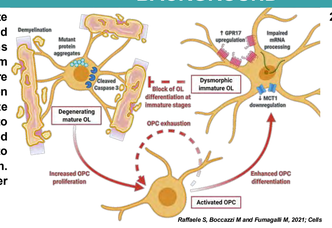


*Raffaele S, Boccazzi M and Fumagalli M, 2021; Cells*

2. **GPR17 regulates OPC differentiation into immature OLs and is downregulated to allow full maturation.**

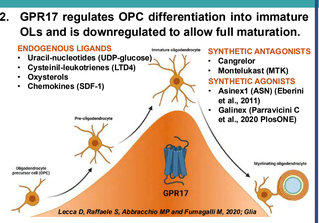


*Lecca D, Raffaele S, Abbracchio MP and Fumagalli M, 2020; Glia*

3. **In the SOD1G93A model, GPR17-overexpressing OPCs expand early and accumulate over time, resulting in reduced mature OLs and impaired maturation. In addition to the efficacy of GPR17 antagonists (Raffaele S. et al., 2024 *BJP*) chronic activation with selective agonists may offer an alternative strategy by promoting receptor desensitization and downregulation, thereby alleviating the differentiation block.**

**Lumbar spinal cord**

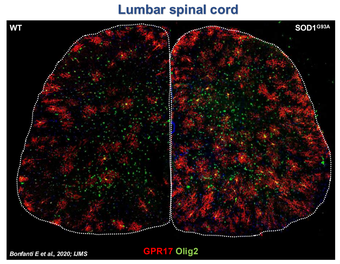


**Mouse spinal cord at P120**

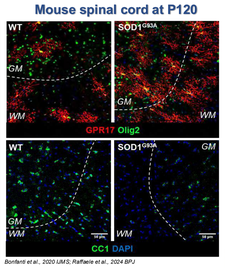


*Bonfanti E. et al., 2020 UMS; Raffaele et al., 2024 BPJ*

**Primary OPC cultures**

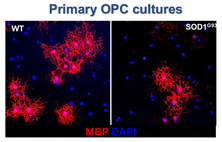


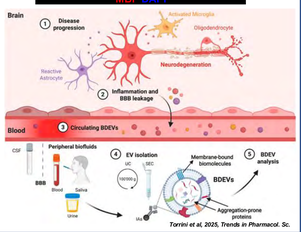


*Torrini et al. 2025, Trends in Pharmacol. Sc.*

4. **Extracellular vesicles (EVs) are lipid bilayer-enclosed particles reflect cellular state and can cross the blood–brain barrier. On this basis, EVs released by OLs, reflecting their reactive state and phenotype, may serve as non-invasive biomarkers to monitor dysfunctional OL dynamics in ALS.**

## AIMS

1. **To validate GPR17 as a therapeutic target, by assessing, in a sex-specific manner, the *in vivo* effects of the selective GPR17 agonist Galinex (GAL) in SOD1$^{G93A}$ mice;**
2. **To track GPR17$^{+}$ OPC expansion and their circulating extracellular vesicles (EVs) during disease progression using our novel GPR17-iCreERT2:GFP/SOD1$^{G93A}$ lineage-tracing mouse.**

## METHODS

### Experimental protocol for aim 1: in vivo assessment of GAL treatment

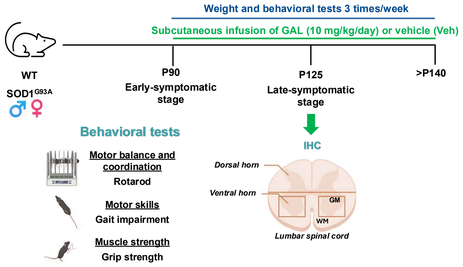


### Pharmacological profile of GAL

*In silico ADME prediction*

| | Recommended range | Compound 9 |
|---|---|---|
| LogP | | 2.68 |
| Number of violations of Lipinski's rule of five | <4 | 0 |
| Number of violations of Jorgensen's rule of three | <3 | 0 |
| Number of property or descriptor value outside the 95% range of similar values for known drugs | 0–5 | 0 |
| Predicted brain/blood partition coefficient | -3.0 - +1–2 | -0.958 |
| [1]MDCK cell permeability in nm/sec | <25 poor | 536 |
| | >500 great | |
| Number of reactive functional groups | 0–2 | 0 |
| Number of likely metabolic reactions | 1–8 | 3 |
| [2]Predicted apparent Caco-2 cell permeability in nm/sec | <25 poor | 446.138 |
| | >500 great | |
| Prediction of the binding to human serum albumin | -1.5 - +1.5 | -0.041 |
| Prediction of human oral absorption | <25% poor | 88.5 |
| | >80% high | |
| Brain penetration sufficient for CNS activity | | yes |
| Absorption across intestinal barrier | | yes |
| Passive absorption across intestinal barrier | | good |
| First-pass metabolism in liver and/or intestine | | no |

*Parravicini C et al., 2020 PLoS One*

[1]MDCK cells are a well-established model for BBB.
[2]Caco-2 cells are a well-established model for the gut-blood barrier.

### Experimental protocol for aim 2: in vivo tracking of GPR17$^{+}$ OPCs and circulating EVs

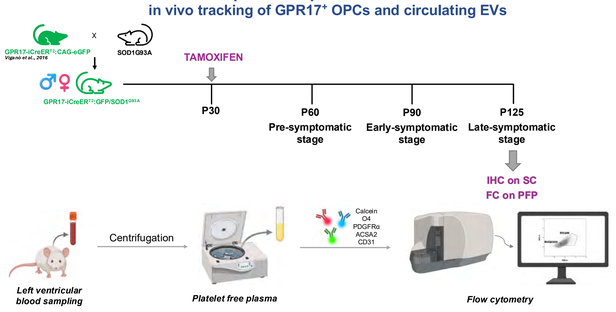


### *In vivo* pharmacokinetics

| Plasma DMPK parameters | 9 |
|---|---|
| Cmax (ng/ml) | 72.3 |
| Tmax (h) | 0.50 |
| Clast (ng/ml) | 4.81 |
| Tlast (h) | 4.00 |
| AUClast (ng·h/ml) | 85.8 |
| t1/2 (h) | 1.09 |

### *Concentration-response curve*

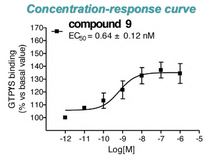


## RESULTS

### 1. Treatment with the selective GPR17 agonist ASN stimulates maturation in primary OPCs from SOD1$^{G93A}$ mice

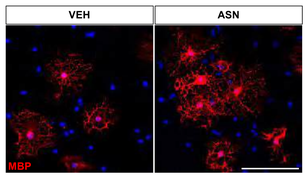


Representative images and quantification of MBP+ mature OLs in SOD1$^{G93A}$ primary cultures exposed to the GPR17 agonist Asinex1 (ASN) or vehicle (VEH). Hoechst33258 was used to label cell nuclei.
n = 9 coverslips from three independent experiments. * p < 0.05, Student's t-test.

### 2. Treatment with the selective GPR17 agonist ASN triggers receptor desensitization and internalization

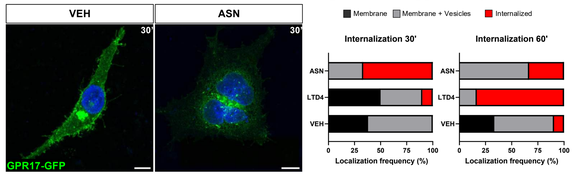


Representative images showing 1321N1 cells transfected with GPR17-GFP reporter and quantification of the percentage of 1321N1 cells with GPR17 localization in the plasma membrane, both membrane and vesicles, or intracellular vesicles after treatment with VEH, the endogenous GPR17 ligand LTD4, the GPR17 agonist ASN, for 30' or 60' during GPR17 internalization assay. n = 5-7 technical replicates from two independent experiments.

### 3. Treatment with the selective GPR17 agonist GAL prolongs survival and delays disease progression of female SOD1$^{G93A}$ mice

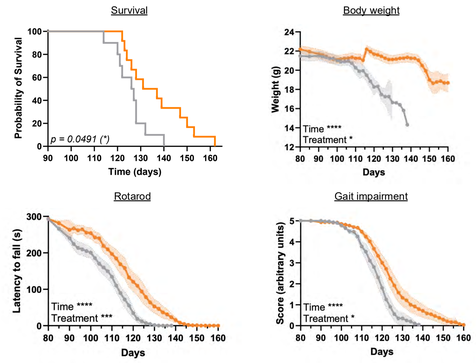


Quantification of survival probability, body weight loss, rotarod performance, gait impairment, and forelimb grip strength of female SOD1$^{G93A}$ mice treated with vehicle (VEH) or the selective GPR17 agonist Galinex (GAL, a brain penetrant compound derived from ASN). n=10-12. Survival was evaluated by Kaplan–Meier analysis with Gehan-Breslow-Wilcoxon test. Body weight and behavior were analyzed by mixed-effects model with Geisser-Greenhouse correction for repeated measures.
* p<0.05, ** p<0.01, *** p<0.001, **** p<0.0001.

### 4.Treatment with selective GPR17 agonist GAL restores OL maturation, fosters myelination and limits MN loss in female SOD1$^{G93A}$ mice

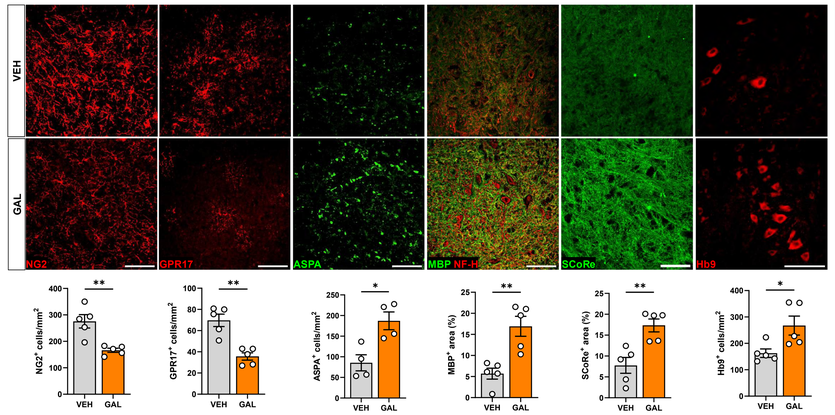


Representative images and quantification of NG2$^{+}$ early OPCs, GPR17$^{+}$ immature OLs, ASPA$^{+}$ mature OLs, MBP$^{+}$NF-H$^{+}$ myelinated axons, SCoRe$^{+}$ compact myelin, and Hb9$^{+}$ MNs in the ventral grey matter of the lumbar spinal cord of P125 female SOD1$^{G93A}$ mice treated with GPR17 selective agonist GAL or VEH. Nuclei were labelled with Hoechst33258. Scale bar: 100 µm. n=4-5 * p<0.05, ** p<0.01, Student's t-test.

### 5. Early and progressive accumulation of GPR17-GFP$^{+}$ OPCs in the spinal cord of GPR17-iCreERT2:GFP/SOD1$^{G93A}$ mice

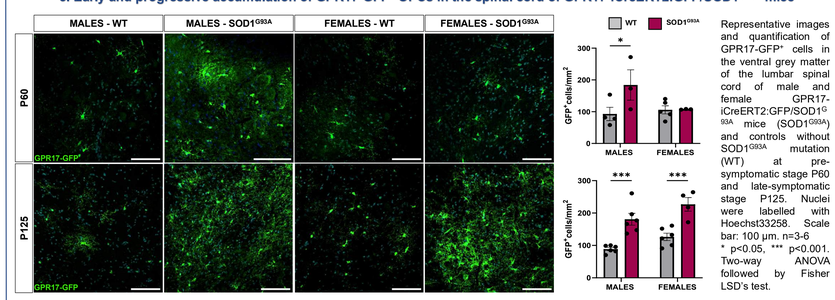


Representative images and quantification of GPR17-GFP$^{+}$ cells in the ventral grey matter of the lumbar spinal cord of male and female GPR17-iCreERT2:GFP/SOD1$^{G93A}$ mice (SOD1$^{G93A}$) and controls without SOD1$^{G93A}$ mutation (WT) at pre-symptomatic stage P60 and late-symptomatic stage P125. Nuclei were labelled with Hoechst33258. Scale bar: 100 µm. n=3-6
* p<0.05, *** p<0.001. Two-way ANOVA followed by Fisher LSD's test.

### 6. Circulating GPR17-GFP+ extracellular vesicles as potential indicators of pathological OPC expansion in the spinal cord of GPR17-iCreERT2:GFP/SOD1G93A mice

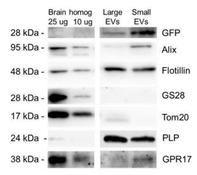


Western Blot analysis of large and small EVs isolated from spinal cord interstitial fluid of GPR17-iCreERT2:GFP mice showing enrichment of GFP and EV markers (Alix, Flotiilin), absence of negative controls (GS28, Tom20), and expression of specific OL lineage markers (PLP, GPR17). Total brain homogeneates from WT mice were used as control.

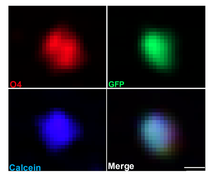


Representative fluorescence images of EVs isolated from plasma of GPR17-iCreERT2:GFP/SOD1$^{G93A}$ mice obtained by confocal microscopy. Intact EVs were labeled with Calcein-AM and are positive for GFP and OL marker O4. Scale bar: 1 µm.

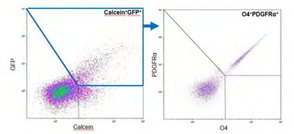


*GFP$^{+}$ EVs expressing OL markers in SOD1$^{G93A}$ mice:*
- ***85.5% O4$^{+}$** (pre-myelinating OLs)*
- ***62.2% PDGFRα$^{+}$** (OPCs)*
- ***52% O4$^{+}$PDGFRα$^{+}$** (immature OLs)*
- *Negative for ACSA2 (astrocytes), CD31 (endotelium)*

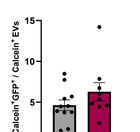


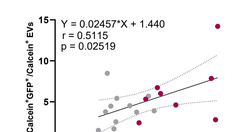


Preliminary flow cytometry analysis of circulating EVs from GPR17-iCreERT2:GFP/SOD1$^{G93A}$ mice (SOD1$^{G93A}$) and controls without SOD1$^{G93A}$ mutation (WT) at late-symptomatic stage P125. Intact EVs were labeled with Calcein-AM. Scatter plots show that a significant fraction of Calcein+GFP+ EVs co-express OL markers O4 and PDGFRα. The histogram shows the quantification of Calcein$^{+}$GFP$^{+}$ EVs fraction, revealing a trend toward increase in SOD1$^{G93A}$ mice compared to WT. Moreover, a positive correlation was found between GFP$^{+}$ cell density in the spinal cord and Calcein$^{+}$GFP$^{+}$ EVs fraction as confirmed by Pearson's correlation test.

### 7. Conserved pathological GPR17 upregulation in post-mortem human spinal cord tissue from ALS cases

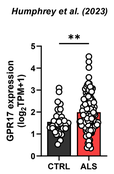


GPR17 expression in post-mortem human lumbar spinal cord from ALS cases and non-neurological disease controls (CTRL), obtained from published bulk RNA-seq datasets (Humphrey et al., 2023, Nat. Neurosc.). CTRL: n = 33; ALS: n = 119. **p < 0.01, Mann–Whitney test.

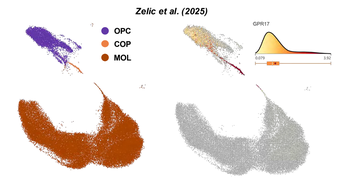


UMAP plots and quantification of GPR17-expressing cells in post-mortem human cervical spinal cord tissue from ALS cases (n = 8) and CTRL (n = 4), derived from published single-nucleus RNA-seq data (Zelic et al., 2025, Immunity). *p < 0.05, Welch's t-test.

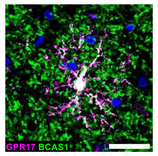


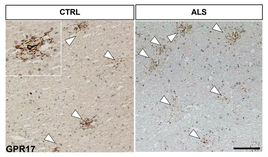


Representative immunofluoroscence images of GPR17 co-localization with the immature oligodendrocyte marker BCAS1 in post-mortem human lumbar spinal cord tissue obtained thanks to the collaboration with Kate Lambertsen Nuclei are counterstained with DAPI. Scale bar: 100 µm.

Representative images and quantification of GPR17$^{+}$ cells (arrowheads) in post-mortem human lumbar spinal cord tissue from ALS cases and CTRL. Scale bar: 100 µm. n = 5 **p < 0.01, Student's t-test.

## CONCLUSIONS & FUTURE PERSPECTIVES

**Treatment with GAL:**
- **Significantly extends survival probability, delays disease progression, and ameliorates motor function of female SOD1$^{G93A}$ mice.**
- **Counteracts pathological GPR17 upregulation and restores OL maturation in the spinal cord of female SOD1$^{G93A}$ mice.**
- **Improves myelination and prevents the loss of MNs in the spinal cord of female SOD1$^{G93A}$ mice.**

**Studies in GPR17-iCreERT2:GFP/SOD1$^{G93A}$ mice:**
- **Reveal increased GPR17$^{+}$ OPC reactivity during disease progression.**
- **Identify OL-derived extracellular vesicles as potential biomarkers of OL pathology in ALS.**

**1. To evaluate GAL effects in rNLS8 mouse model of TDP-43 proteinopathy**

**2. To validate oligodendroglial EVs as potential biomarkers in ALS patients.**


*Projects GPR17-ALS (2019) and DORALS (2025) to MF*

# JAK family inhibitors rescue cytoplasmic dsRNA-driven TDP43 mislocalization in human iPSC-derived neurons

**Sutapa Som Chaudhury**[1,2], Himanish Basu[3], Caitlin Mills[2], Christine Marques[1], Rohan Bhukar[1,2], Mark Appleman[1], Clotilde Lagier-Tourenne[1], Brian J. Wainger[1], Isaac M. Chiu[3]*, Mark W. Albers[1,2]*

[1]Department of Neurology, Massachusetts General Hospital, Charlestown, MA 02129; [2]Laboratory of Systems Pharmacology, Harvard Program in Therapeutic Science, Harvard Medical School, Boston, MA 02115; [3]Department of Immunology, Harvard Medical School, 77 Avenue Louis Pasteur, Boston, MA 02215.

## Abstract

**Background:** The cytoplasmic inclusions of TDP43 are a hallmark of 97% of ALS cases. Cytoplasmic dsRNA (cdsRNA) is spatially coincident with TDP43 inclusions in ALS brains. We hypothesized that cdsRNA drives TDP43 mislocalization, leading to an innate immune response in cultured human iPSC (hiPSC)-derived NGN2 cortical neurons with an ALS-causing TDP43 mutation.

**Methods:** HiPSC-derived, TDP43-G298S+/- NGN2 cortical and isogenic control lines were treated with dsRNA mimetic named polyinosinic:polycytidylic acid (polyIC). Neuronal cell survivability (CellTiter-Glo (CTG)) and neurite tracking were measured. We quantified the mislocalization of nuclear TDP43 and its coincidence with the cdsRNA using confocal microscopy and a customized script. We treated cells with JAK and TYK2 inhibitors in the presence of dsRNA mimetic. Meso Scale Discovery (MSD) assays were used to quantify the cytokines CXCL10 and CCL2.

**Results:** The dsRNA mimetic potentiated both cell death and neurite loss in TDP43 mutant cells relative to isogenic control cells. The ED25 dose of the dsRNA mimetic was 2 µg/ml. In contrast, the cGAS-STING agonist (cGAMP) did not potentiate cell death in either TDP43 mutant or isogenic control lines. We observed TDP43 mislocalization and its coincidence with cdsRNA using confocal microscopy, suggesting that cdsRNA can drive TDP43 mislocalization. Both CXCL10 and CCL2 levels were increased with dsRNA mimetic induction, consistent with the neuroimmune response seen in brain tissue and patient CSF samples. Interestingly, treatment with either JAK inhibitor Ruxolitinib or the TYK2 inhibitor Deucravacitinib rescued TDP43 mislocalization, cell death, neurite outgrowth, and cytokine release.

**Summary:** cdsRNA-driven TDP43 mislocalization leading to innate immune activation in an ALS-causing TDP43 mutant differentiated iPSC neurons was reversed by JAK and TYK2 inhibitors.

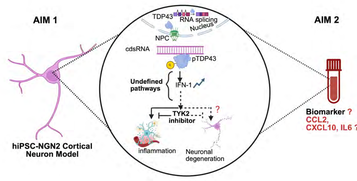


**Figure 1: Graphical abstract summarizing the aims of the study. Aim 1:** JAK/TYK2 inhibitor effects on hiPSC-neuron cell death and TDP43 localization. **Aim 2:** Meso Scale Discovery (MSD) of Inflammatory biomarkers downstream of JAK/TYK2 activation.

## cdsRNA accumulation in different ALS-causing mutant hiPSC-derived NGN2 neurons

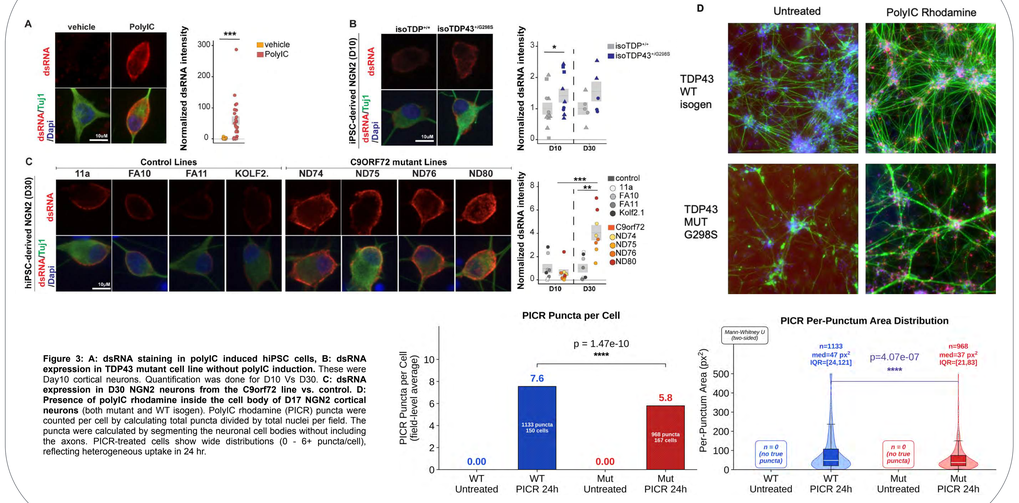


**Figure 3: A: dsRNA staining in polyIC induced hiPSC cells, B: dsRNA expression in TDP43 mutant cell line without polyIC induction.** These were Day10 cortical neurons. Quantification was done for D10 Vs D30. **C: dsRNA expression in D30 NGN2 neurons from the C9orf72 line vs. control. D: Presence of polyIC rhodamine inside the cell body of D17 NGN2 cortical neurons** (both mutant and WT isogen). PolyIC rhodamine (PICR) puncta were counted per cell by calculating total puncta divided by total nuclei per field. The puncta were calculated by segmenting the neuronal cell bodies without including the axons. PICR-treated cells show wide distributions (0 - 6+ puncta/cell), reflecting heterogeneous uptake in 24 hr.

## JAK family inhibitors rescue TDP43 mislocalization in RenVM and WT NGN2 neurons

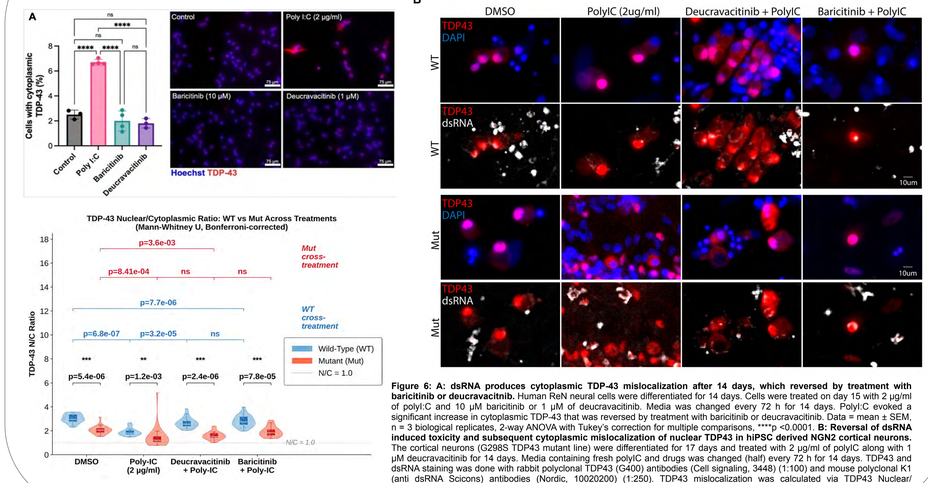


**Figure 6: A: dsRNA produces cytoplasmic TDP-43 mislocalization after 14 days, which reversed by treatment with baricitinib or deucravacitinib.** Human ReN neural cells were differentiated for 14 days. Cells were treated on day 15 with 2 µg/ml of poly:C and 10 µM baricitinib or 1 µM of deucravacitinib. Media was changed every 72 h for 14 days. Poly:C evoked a significant increase in cytoplasmic TDP-43 that was reversed by treatment with baricitinib or deucravacitinib. Data = mean ± SEM, n = 3 biological replicates, 2-way ANOVA with Tukey's correction for multiple comparisons, ****p <0.0001. **B: Reversal of dsRNA induced toxicity and subsequent cytoplasmic mislocalization of nuclear TDP43 in hiPSC derived NGN2 cortical neurons.** The cortical neurons (G298S TDP43 mutant line) were differentiated for 17 days and treated with 2 µg/ml of polyIC along with 1 µM deucravacitinib for 14 days. Media containing fresh polyIC and drugs was changed (half) every 72 h for 14 days. TDP43 and dsRNA staining was done with rabbit polyclonal TDP43 (G400) antibodies (Cell signaling, 3448) (1:100) and mouse polyclonal K1 (anti dsRNA Scicons) antibodies (Nordic, 10020200) (1:250). TDP43 mislocalization was calculated via TDP43 Nuclear/ Cytoplasmic ratio (Mann-Whitney U, Bonferroni corrected, ***p<0.001, **p<0.01, *p<0.05 and ns p>0.05).

## Introduction

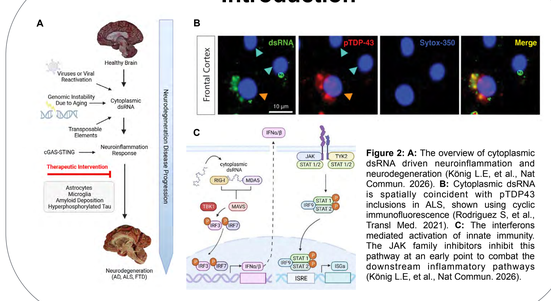


**Figure 2: A:** The overview of cytoplasmic dsRNA driven neuroinflammation and neurodegeneration (König L.E, et al., Nat Commun. 2026). **B:** Cytoplasmic dsRNA is spatially coincident with pTDP43 inclusions in ALS, shown using cyclic immunofluorescence (Rodriguez S, et al., Transl Med. 2021). **C:** The interferons mediated activation of innate immunity. The JAK family inhibitors inhibit this pathway at an early point to combat the downstream inflammatory pathways (König L.E, et al., Nat Commun. 2026).

## Cytoplasmic dsRNA induced greater neuronal cell death in a TDP43 mutant (G298S) line relative to its wild type isogenic control line

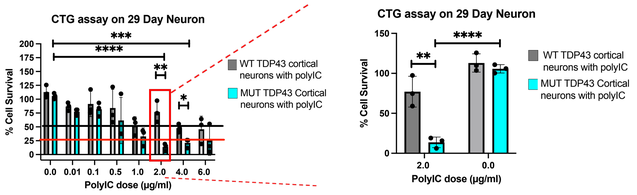


**Figure 4: TDP-43 mutant iPSCs are more vulnerable to dsRNA relative to wild type iPSC-derived neurons.** TDP-43 mutant and isogenic control iPSC-derived NGN2 cortical neurons were differentiated and treated with 2 µg/ml of polyIC on day 17. Media containing fresh polyIC was changed every 72 h for 12 days. Cell viability was assessed by Cell Titer Glo (CTG) assay, normalized to vehicle control. Significant differences were observed between WT and mutant TDP-43 cells treated with 2 µg/ml polyIC and between Data = mean ± SEM, n = 3 biological replicates, unpaired t-test, *p<0.04, **p<0.005, ****p<0.0001.

## TYK2 and JAK family inhibitors reduce CXCL10 and CCL2

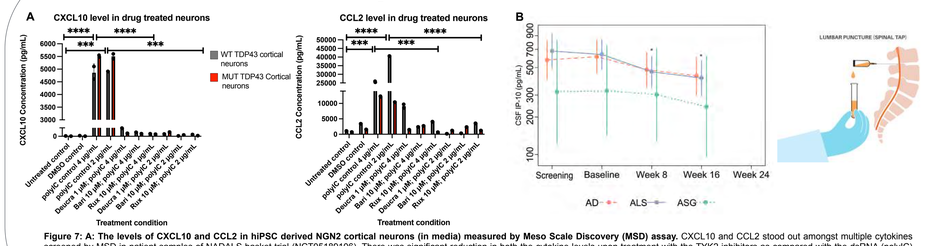


**Figure 7: A: The levels of CXCL10 and CCL2 in hiPSC derived NGN2 cortical neurons (in media) measured by Meso Scale Discovery (MSD) assay.** CXCL10 and CCL2 stood out amongst multiple cytokines screened by MSD in patient samples of NADALS basket trial (NCT05189106). There was significant reduction in both the cytokine levels upon treatment with the TYK2 inhibitors as compared with the dsRNA (polyIC) induced control. ***p and ****p<0.0001 (N=3) calculated via unpaired t-test. **B: CXCL10 levels normalized to baseline i.e., at week 8 with no drug.** All patients received 2mg/day oral Baricitinib in the 8-week duration between the baseline and week 8 visit as well as 4mg/day oral Baricitinib in the 8-week duration between the week 8 and week 16 visits. No drug was given in the 8 weeks between screening (week 0) and baseline (week 8) to evaluate the stability of the biomarker over time. Reduction in CXCL10 after the baseline visit in all 7 patients can be used as evidence for JAK inhibitor-mediated reduction in CXCL10 in the CSF. The level of significances was calculated (N=7) by the Friedman test (Dunn's multiple comparisons test); *p<0.02, **p<0.002.

## Methods

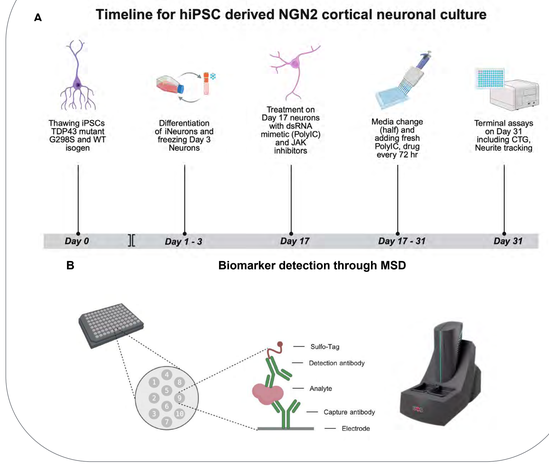


## Contact Information

ssomchaudhury@bwh.harvard.edu;
albers.mark@mgh.harvard.edu

## TYK2 and JAK family inhibitors rescue neuronal cell death

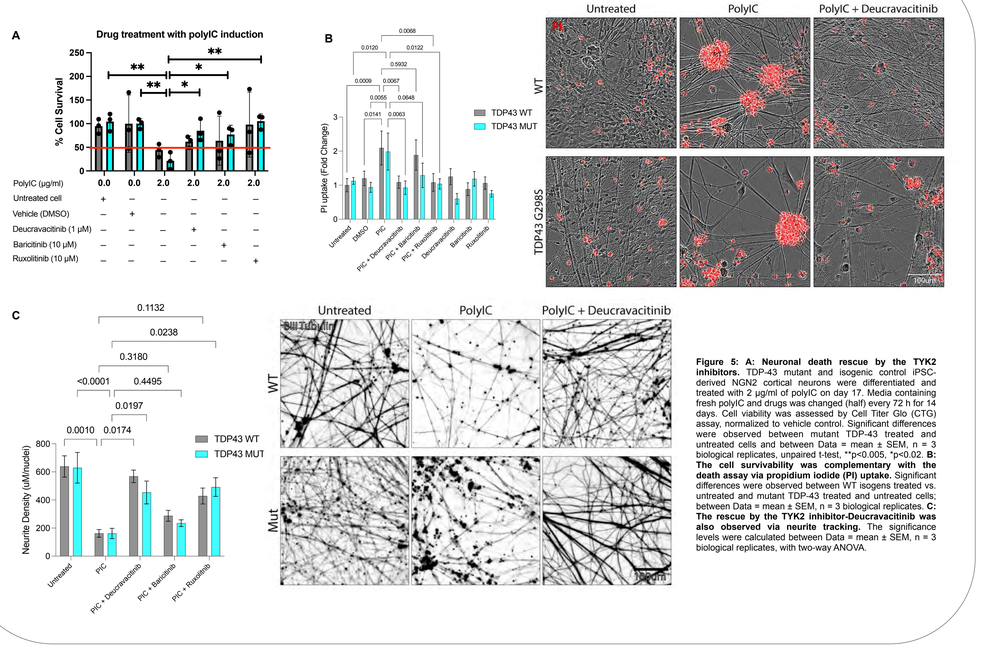


**Figure 5: A: Neuronal death rescue by the TYK2 inhibitors.** TDP-43 mutant and isogenic control iPSC-derived NGN2 cortical neurons were differentiated and treated with 2 µg/ml of polyIC on day 17. Media containing fresh polyIC and drugs was changed (half) every 72 h for 14 days. Cell viability was assessed by Cell Titer Glo (CTG) assay, normalized to vehicle control. Significant differences were observed between mutant TDP-43 treated and untreated cells and between Data = mean ± SEM, n = 3 biological replicates, unpaired t-test, **p<0.005, *p<0.02. **B: The cell survivability was complementary with the death assay via propidium iodide (PI) uptake.** Significant differences were observed between WT isogens treated vs. untreated and mutant TDP-43 treated and untreated cells; between Data = mean ± SEM, n = 3 biological replicates. **C: The rescue by the TYK2 inhibitor-Deucravacitinib was also observed via neurite tracking.** The significance levels were calculated between Data = mean ± SEM, n = 3 biological replicates, with two-way ANOVA.

## Conclusions

1. Our preliminary findings indicate cdsRNA is a stressor that can induce TDP43 mislocalization in differentiated human neural cells and hiPSC-derived NGN2 neurons.
2. JAK family inhibitors prevent human neural cell and cortical neuronal death and TDP43 mislocalization induced by cdsRNA.
3. Further studies are directed at elucidating the mechanistic connection between JAK family inhibition with TDP43 mislocalization, neuroinflammation, and neural cell death in cellular and mouse models and in the proteomic data from the recently completed NADALS basket trial (NCT05189106).

## References

1. Rodriguez S, et al. Genome-encoded cytoplasmic double-stranded RNAs, found in C9ORF72 ALS-FTD brain, propagate neuronal loss. Sci Transl Med. 2021 Jul 7;13(601). PubMed ID: 34233951
2. Rodriguez S, et al. Machine learning identifies candidates for drug repurposing in Alzheimer's disease. Nat Commun. 2021 Feb 15;12(1):1033. PMID: 33589615
3. Dunker W, et al. TDP-43 prevents endogenous RNAs from triggering a lethal RIG-I-dependent interferon response. Cell Rep. 2021; 35.
4. Saldi T.K, et al. TDP-1, the Caenorhabditis elegans ortholog of TDP-43, limits the accumulation of double-stranded RNA. EMBO J. 2014; 33(2947–2966).
5. Klim JR, et al. ALS-implicated protein TDP-43 sustains levels of STMN2, a mediator of motor neuron growth and repair. Nat Neurosci. 2019 Feb;22(2):167-179. PMID: 30643292
6. König L.E, et al. TYK2 mediates neuroinflammation in Alzheimer's disease brains with TDP-43 pathology. Nat Commun. 2026 March 14.

## Acknowledgements

The authors thank all the patients who donated brain tissue and bio fluids to the study. This work was funded by the Target ALS grant, 'Neuronal innate immune pathways that drive cell death and inflammation in ALS', and NADALS trial (NCT05189106).

# A postmortem whole human brain platform for CNS drug discovery

Congwei Wang, Nghia Nguyen, Scott Pope, Machele Riccio, Josip Butkovic, Ivan Mumlek, Chunmin Ge, Raghav Kansal, Leah Rosales, Lindsay Slupczewski, Lucija Barisic, Brad Parry, Sean Murphy, Zvonimir Vrselja, Paul D. Wes

Bexorg, New Haven, CT, USA

## INTRODUCTION

A major barrier to developing effective therapies for Alzheimer's disease is the limited ability of preclinical models to predict clinical efficacy. Animal models often fail to recapitulate key aspects of human disease biology and etiology, and human-derived in vitro systems, while valuable, typically lack the multicellular architecture and mature phenotypes of the adult aged brain. To address this gap, we established BrainEx, an ex vivo whole brain perfusion platform that supports physiological maintenance of molecular and cellular function in postmortem human brains, including tissue from donors with Alzheimer's disease. BrainEx enables preclinical drug discovery and translational validation directly in the human disease brain, supporting target validation, pharmacokinetic assessment and brain penetration, pharmacodynamic and functional readouts, biomarker discovery, and novel target identification.

## ETHICAL CONSIDERATIONS

Acquisition of postmortem human brains adheres to the highest possible ethical standards, overseen by an independent board of world-renowned bioethicists. Brains are procured through Organ Procurement Organizations (OPOs) with enhanced levels of consent from patients and families that specifically cover the BrainEx platform. Measures are taken on the BrainEx device to ensure that there is no possibility of coordinated network activity associated with consciousness.

## [1] THE BRAINEX PLATFORM

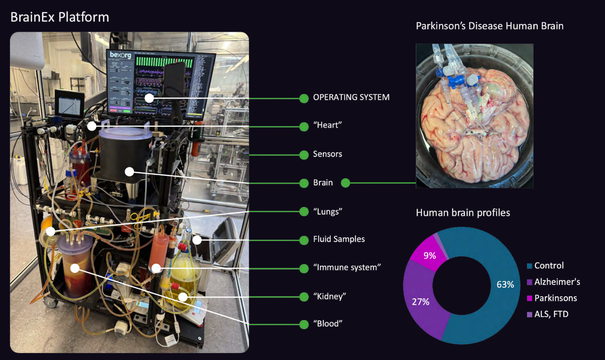


**Figure 1. The BrainEx platform enables drug discovery in whole human disease brains.** Bexorg has established a platform that maintains intact, molecularly and cellularly active postmortem human brains. The brain is connected to the BrainEx device via its endogenous vascular system. An acellular artificial perfusate supplies the brain with oxygen and nutrients, while a real-time operating system regulates physiological homeostasis. Drugs can be administered to the brain systemically, and pharmacokinetics, pharmacodynamics, and functional pharmacology can be assessed longitudinally in brain tissue and translational biofluids.

## [2] BEX-001 PROGRAM - RESTORING MITOCHONDRIA-LINKED BIOENERGETICS IN NEURODEGENERATION

*Metabolic pathway of interest:*

***Efficacy Biomarker A ⟶ Efficacy Biomarker B***

***+ATP (Energy)***

Neurodegeneration is increasingly associated with impaired bioenergetics, including mitochondrial dysfunction, reduced metabolic flexibility, and diminished ATP-generating capacity. In Alzheimer's disease and other neurodegenerative disorders, these deficits are thought to contribute directly to synaptic dysfunction, cellular stress, and progressive loss of neuronal resilience. BEX-001 is a small molecule designed to modulate a key mitochondria-linked bioenergetic pathway in human brain tissue. We hypothesized that pharmacologic engagement of this pathway would enhance metabolic activity and generate a measurable pharmacodynamic and biomarker response, with the greatest effects in neurodegeneration-affected brains.

References

Daniele, S. G., Trummer, G., Hossmann, K. A., et al. (2021). Brain vulnerability and viability after ischaemia. Nature Reviews Neuroscience, 22, 553–572. https://doi.org/10.1038/s41583-021-00488-y

Andrijevic, D., Vrselja, Z., Lysyy, T., et al. (2022). Cellular recovery after prolonged warm ischaemia of the whole body. Nature, 608, 405–412. https://doi.org/10.1038/s41586-022-05016-1

Vrselja, Z., Daniele, S. G., Silbereis, J., et al. (2019). Restoration of brain circulation and cellular functions hours post-mortem. Nature, 568, 336–343. https://doi.org/10.1038/s41586-019-1099-1

## [3] DEMOGRAPHICS


**Figure 2. Demographic characteristics of the BrainEx BEX-001 donor cohort.** Cohort summary statistics are shown above (n = 58; 32 male, 26 female; median age, 79 years). Plots show the distributions of sex, age, BMI, and race/ethnicity across donors.

## [4] PHARMACOKINETICS (PK)


**Figure 3. Pharmacokinetics of BEX-001 on the BrainEx platform.** BEX-001 (0.6 µg/mL) or vehicle control was administered systemically via the BrainEx perfusate circuit and quantified longitudinally over 12 h by LC-MS in circulating perfusate (ng/mL) (left) and prefrontal cortex (PFC) tissue (ng/g) (right). BEX-001 administration in the perfusate resulted in full bioavailability in the circulating perfusate (left) and gradually redistributed into the brain (right). At 6 h, a washout step was initiated, clearing BEX-001 from the perfusate (left). Drug concentration in brain tissue subsequently decreased, though a substantial drug depot remained in the brain (right).

## [5] PHARMACODYNAMICS (PD)

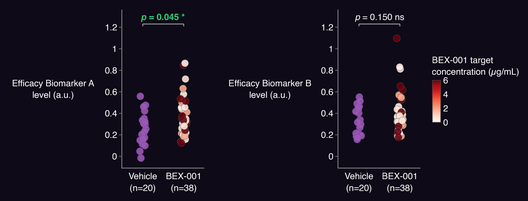


**Figure 4. Efficacy of BEX-001 in BrainEx-perfused human brains.** BEX-001 or vehicle was delivered through the BrainEx perfusate, and efficacy biomarker levels were compared across all human brains. Each point represents one perfusion run/brain (vehicle, n = 20; BEX-001, n = 38), with BEX-001 samples colored by target concentration (0 – 6 µg/mL). BEX-001 significantly increased Efficacy Biomarker A (p = 0.045) but did not alter Efficacy Biomarker B (p = 0.150, ns).

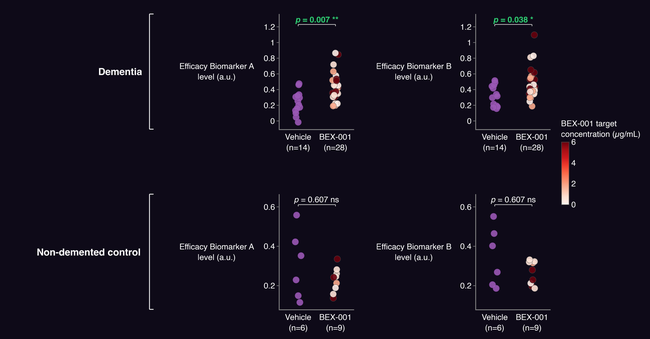


**Figure 5. Clinical diagnosis stratifies the efficacy of BEX-001 in BrainEx-perfused human brains.** In dementia brains, BEX-001 significantly increased Efficacy Biomarker A and Efficacy Biomarker B versus vehicle, whereas neither biomarker changed significantly in non-demented controls. Each point represents one perfusion run/brain, with BEX-001 samples colored by achieved target concentration (0 – 6 µg/mL).

## [6] MECHANISM OF ACTION

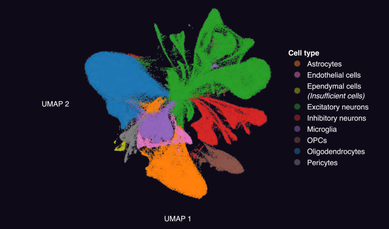


**Figure 6. Single-nucleus RNA sequencing of post-perfusion human brain tissue identifies cell-type-specific transcriptional responses to BEX-001.** Brain tissue collected after BEX-001 or vehicle perfusion was profiled by snRNA-seq. Top, UMAP of nuclei colored by annotated major brain cell types, defining the cellular landscape of the post-perfusion tissue. Bottom, cell-type-specific volcano plots comparing BEX-001- versus vehicle-treated samples in representative populations (excitatory neurons, astrocytes, and microglia), displayed as log2 fold change versus −log10 adjusted p-value. The top 10 upregulated genes in each cell type are highlighted in red.

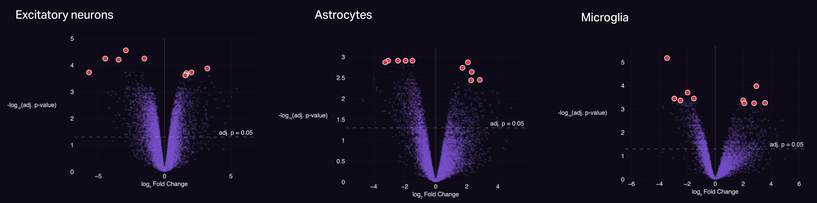


## [7] TRANSLATIONAL BIOMARKERS

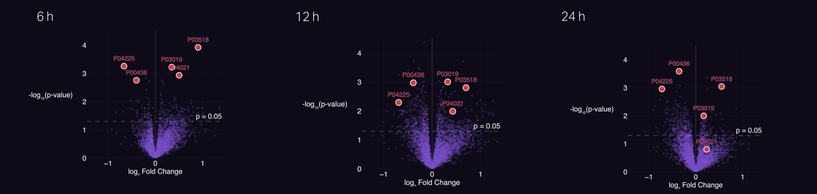


**Figure 7. Time-resolved volcano plots of perfusate proteomics after BEX-001 treatment.** Differential protein expression between BEX-001 and vehicle was assessed in BrainEx perfusate at 6, 12, and 24 h using SomaScan 11K. Each plot displays log2 fold change versus −log10(p-value), with candidate panel proteins highlighted in red and the nominal significance threshold marked at p = 0.05. The data reveal time-dependent and recurring candidate biomarkers of BEX-001 response in translational biofluids.

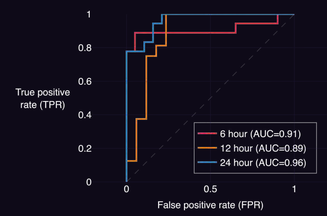


**Figure 8. Longitudinal perfusate proteomics identifies a BEX-001-responsive biomarker signature.** Machine-learning classifiers trained on proteomic profiles from translational biofluid (perfusate) samples collected at 6, 12, and 24 h during BrainEx perfusion discriminated BEX-001 from vehicle with high accuracy (AUC = 0.91, 0.89, and 0.96, respectively). The dashed diagonal line indicates chance performance (AUC = 0.5).

## SUMMARY

BrainEx enables translational CNS drug discovery directly in intact postmortem human brains by supporting longitudinal assessment of drug exposure, pharmacology, and biomarker response in native human tissue. In the BEX-001 program, systemic delivery through the perfusate achieved full bioavailability in circulation, gradual redistribution into the prefrontal cortex, and a persistent tissue depot after a 6-hour washout, demonstrating sustained brain exposure on the platform. Pharmacodynamically, BEX-001 increased Efficacy Biomarker A across all brains and, when stratified by clinical diagnosis, significantly increased both Efficacy Biomarker A and Efficacy Biomarker B in dementia brains, while no significant effects were observed in non-demented controls. Longitudinal perfusate proteomics identified a robust treatment-responsive biomarker signature, with machine-learning classifiers distinguishing BEX-001 from vehicle with high accuracy across 6, 12, and 24 hours. In parallel, single-nucleus RNA sequencing of post-perfusion tissue revealed cell-type-specific transcriptional responses to BEX-001. Together, these findings show that BrainEx can simultaneously measure PK, disease-relevant pharmacology, and translational biomarkers in the human brain, supporting BEX-001 as a promising modulator of mitochondria-linked bioenergetics in neurodegeneration.

# The ALS Global Research Initiative (AGRI)

Laura Dugom1, Daniel Weatherill1,Amy Easton1, Lizzi Neylon10, Kaycie Opiyo3, Michael Weiss3, Aeryn Hopwood4, Senda Ajroud-Driss4, Lada Filippov5, James Berry5, Huy Tran6, Bjorn Oskarsson6, Kyra Nagle, Cindy Ly7, Gilbert Gutierrez8, John Ravits8, Benjamin Hoover9, Christina Wing9, Matthew Harms9, Neil Shneider9, Whitney Dailey10, Shafeeq Ladha10, Cassandra Holmes11, Shakti Nayar11, Brent Harris11, Sarah Berth12, Jorge Zaragoza Zapiain12,Frances Aponte13, Brenda Deliz13, Valerie Wojna13, Manuela Quiroga Carillo14, Martha Peña14, Marc Gotkine15, Lina Abd Alhalim15, Seok-jin Choi16, Manish Raisinghani1, Robert Bowser2, 10

1 Target ALS, New York, New York, USA 2 Department of Translational Neuroscience, Barrow Neurological Institute, Phoenix, AZ, USA 3 Department of Neurology, University of Washington, WA, USA 4 Department of Neurology, Northwestern University, Chicago, IL, USA 5 Department of Neurology, Massachusetts General Hospital, Boston, MA, USA 6 Department of Neurology, Mayo Clinic Jacksonville, Jacksonville, FL, USA 7 Department of Neurology, Washington University St. Louis, St. Louis, MO. USA 8 Department of Neurosciences, University of California, San Diego, San Diego, CA, USA 9 Department of Neurology, Columbia University Medical Center, New York NY, USA 10 Department of Neurology, Barrow Neurological Institute, Phoenix, AZ, USA 11 Department of Neurology and Pathology, Georgetown University, Washington, DC, USA 12 Baylor College of Medicine, Waco, TX, USA 13 University of Puerto Rico, San Juan, Puerto Rico 14 Instituto Roosevelt, Bogotá, Colombia 15 Hebrew University, Jerusalem, Israel 16 Seoul National University Hospital, Seoul, South Korea 17 Henrik Zetterberg Lab

## Background

ALS is a devastating neurodegenerative disease affecting motor neurons, with causes that remain largely unknown. To accelerate discovery and therapeutic development, Target ALS launched the ALS Global Research Initiative (AGRI), an international effort generating deeply characterized clinical, molecular, and environmental datasets and sharing them through the Target ALS Data Engine, an open science research platform. AGRI integrates two complementary observational studies: the Global Natural History Study (GNHS), a longitudinal study collecting clinical data and biospecimens from people living with ALS and healthy controls, and a community outreach study (CBOS) conducting one time visits to capture environmental exposures and long read genomic data. Together, AGRI aims to build a diverse global dataset to study disease risk, progression, and therapeutic targets.

## Methods

The GNHS is an international longitudinal study currently across 15 sites with continued expansion in North and South America and Asia. Participants with ALS complete in clinic visits every 4 months for up to 16 months,including neurological exams, ALSFRS R scoring, cognitive testing, and collection of blood, urine, and cerebrospinal fluid. Biospecimens are analyzed using whole genome sequencing, proteomics, and neurofilament light assays along with clinical, environmental, and digital health data. The CBOS complements GNHS through one time visits in communities with limited access to research participation, streamlining clinical assessments, questionnaires, and blood collection to broaden inclusion in ALS research. Data from both studies are available in the Target ALS Data Engine, enabling integrated analyses across longitudinal and community based cohorts.

## Results

To date, 330 participants have enrolled in the Global Natural History Study (GNHS) and 101 in the Community Based Outreach Study (CBOS). AGRI has generated longitudinal clinical, digital health, and multiomic datasets, with more than 42,000 biofluid samples available in the biorepository. GNHS data spans eight modalities with over 75% of participants contributing to three or more data types. A total of 180 long read whole genome sequences have been generated from (99 from CBOS and 81 from GNHS), with the aim of reaching 6,000 long read sequences. Initial analyses of 150 participants (126 ALS and 88 Non-neurological Control participants) demonstrate disease progression over time as measured by ALSFRS R scores. The Target ALS Data Engine supports 579 investigators across 34 countries analyzing AGRI datasets. Increasing genetic diversity is evident, with non-European ancestry rising to 33% in AGRI participants, highlighting the value of geographically and ethnically diverse data.

## Conclusion

AGRI establishes a global framework for ALS research by integrating longitudinal clinical data, multi-omic profiling, and open data sharing. Through the Target ALS Data Engine, AGRI creates a scalable resource that accelerates biomarker discovery, deepens understanding of disease heterogeneity, and supports the development of more effective therapies

## AGRI: A Framework for Global ALS Research

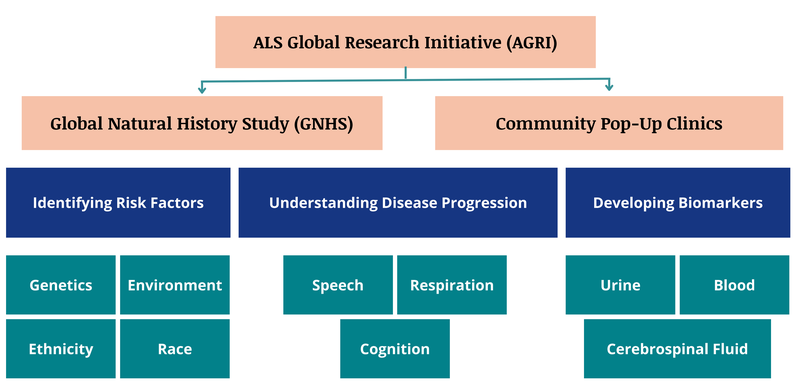


## AGRI Enrollment

**The table is based on data that has been entered, not total enrolled.

| | ALS | | Control | | Total | |
|---|---|---|---|---|---|---|
| | Male | Female | Male | Female | Male | Female |
| GNHS | 104 | 76 | 69 | 58 | 173 | 134 |
| CBOS | 15 | 14 | 21 | 51 | 36 | 65 |
| AGRI Total | 119 | 90 | 90 | 109 | 209 | 199 |

## Study Designs: Longitudinal and Community-Based Approaches

### Global Natural History Study

**Participants**

**Clinic Visits**

**ALS:**
5 visits
0, 4, 8, 12, 16 mos

**HC:**
2 visits
0, 12 mos

- ALSFRS-R/Harmonized
- SVC
- Neurologic Exam
- ALS-CBS/ECAS
- Medications
- Family History
- Environmental Questionnaire

CSF Plasma Serum Urine

**Optional At Home Assessments**
(every 2 weeks)

**Speech and Motor Function Measures**

Aural Analytics
**100 ALS, 50 HC**
COMPLETED

modality.ai
**100 ALS, 50 HC**

**Respiratory Measures**

ZEPHYR
**100 ALS and HC**
COMPLETED

### Community-Based Clinics

**Participants**

**Pop-Up or Community Site**
One time visit for ALS and control participants

- Informed Consent
- Self reported ALSFRS
- Self reported ALS history and diagnosis
- Epidemiological and environmental questionnaire

Whole Blood

## Data Engine

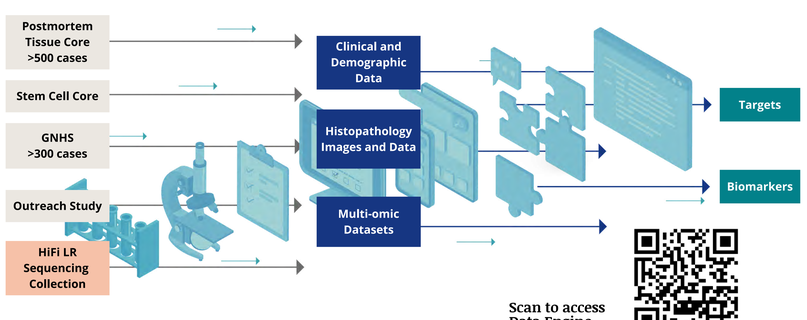


## Tables

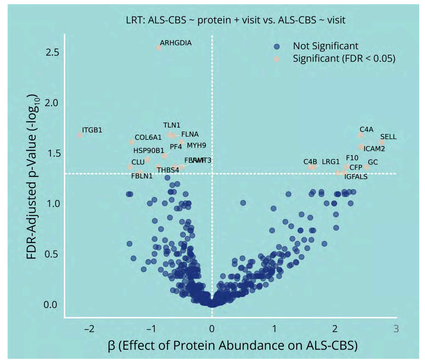


### Plasma Proteins Associated with ALS-CBS Cognitive Subscore in ALS Subjects

No significant associations were observed in CSF, but ~2 dozen plasma proteins were significantly associated with ALS-CBS cognitive subscore in linear mixed models. These include focal adhesion components (e.g., integrin β1, talin, filamin, kindlin), complement regulators (e.g., clusterin, C4A/C4B), and adhesion molecules (e.g., L-selectin, ICAM2), implicating adhesion signaling and neuroinflammatory pathways.

### Distribution of ALS-CBS Cognitive Subscores in ALS Subjects within GNHS

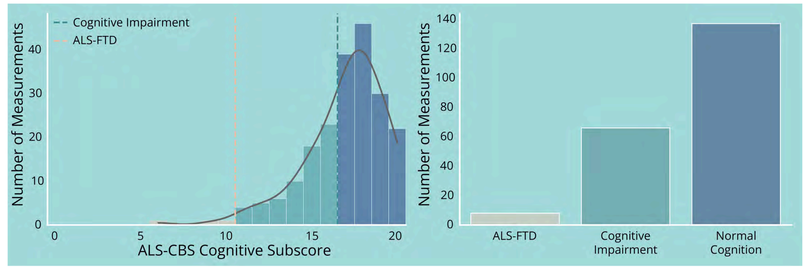


Most participants show normal cognition; smaller subsets exhibit ALS–FTD–like or intermediate (mild) impairment, highlighting cognitive heterogeneity in ALS.

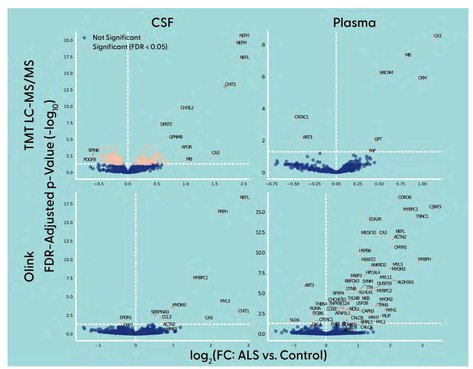


### Proteomics Differential Expression

Across TMT mass spectrometry and Olink platforms in both CSF and plasma, ALS participants exhibit clear proteomic differences relative to controls. Differential expression analyses consistently identify biologically meaningful disease signals, including neuronal injury markers (neurofilament proteins), synaptic adhesion molecules (neurexins, contactins), and neuroinflammatory markers (CHI3L1, complement proteins). Together, these findings confirm that multi-platform proteomics datasets capture robust, disease-relevant molecular signatures in ALS.

## Acknowledgments

Thank you to our partners.

ALS Arizona
DNASTACK
verily

# The Target ALS Global Natural History Study: Unbiased 35-plex TMTpro-MS proteomics to accelerate biofluid biomarker and drug target discovery in amyotrophic lateral sclerosis

Daisuke Yasui[1], Daniel Weatherill[3], Laura Dugom[3], Hayder Shweliyya[16], Kaycie Opiyo[4], Michael Weiss[4], Emma Schmidt[5], Senda Ajroud-Driss[5], Reba Glory Cabral[6], James Berry[6], Huy Tran[7], Bjorn Oskarsson[7], Kyra Nagle[1], Timothy Miller[1], Gilbert Gutierrez[8], John Ravits[8], Benjamin Hoover[9], Matthew Harms[9], Neil Shneider[9], Lizzi Neylon[2], Whitney Dailey[2], Shafeeq Ladha[2], Cassandra Holmes[10], Joseph Lee[10], Nicholas Streicher[10], Shakti Nayar[10], Brent Harris[10], Jorge Zaragoza Zapiain[11], Sarah Berth[11], Frances Aponte[12], Brenda Deliz[12], Valerie Wojna[12], Manuela Quiroga Carillo[13], Martha Peña[13], Lina Abd Alhlim[14], Marc Gotkine[14], Lee Jiwon[15], Choi Jiwon[15], Seok-Jin Choi[15], Manish Raisinghani[3], Henrik Zetterberg[16], Johan Gobom[16], Amy Easton[3], Robert Bowser[2]*, Cindy V. Ly[1]*

**Affiliations**

1 Department of Neurology, Washington University St. Louis, St. Louis, MO, USA 2 Departments of Translational Neuroscience and Neurology, Barrow Neurological Institute, Phoenix, AZ, USA 3 Target ALS, New York, NY, USA 4 Department of Neurology, University of Washington, WA, USA 5 Department of Neurology, Northwestern University, Chicago, IL, USA 6 Department of Neurology, Massachusetts General Hospital, Boston, MA, USA 7 Department of Neurology, Mayo Clinic Jacksonville, Jacksonville, FL, USA 8 Department of Neurosciences, University of California, San Diego, San Diego, CA, USA 9 Department of Neurology, Columbia University Medical Center, New York, NY, USA 10 Department of Neurology and Pathology, Georgetown University, Washington, DC, USA 11 Baylor College of Medicine, Waco, TX, USA 12 University of Puerto Rico, San Juan, Puerto Rico 13 Instituto Roosevelt, Bogotá, Colombia 14 Hebrew University, Jerusalem, Israel 15 Seoul National University Hospital, Seoul, South Korea 16 University of Gothenburg, Sweden

**Email Contact:**
**d.yasui@wustl.edu**

## Background & Objective

Amyotrophic lateral sclerosis (ALS) is a fatal, rapidly progressive neurodegenerative disease of motor neurons weakness, muscle atrophy, respiratory failure, and death within 2-5 years of symptom onset. Diagnosis is often delayed by nearly a year after symptom onset and therapeutics are limited. Thus, improved biomarkers are needed to accelerate early diagnosis, monitor disease progression, and uncover novel therapeutic pathways. Although neurofilaments (NfL and pNfH) and chitinases (e.g., CHIT1, CHI3L2) measured in bliofluids have been shown to serve as proxies of neurodegeneration and neuroinflammation[3], further identification of disease- and pathway-specific biomarker signatures are warranted. Advanced proteomic platforms and mass spectrometry have demonstrated of cerebrospinal fluid (CSF) and plasma have highlighted the potential of biofluid biomarkers to capture both central and systemic ALS pathology[1,2]

We utilized state-of-the-art 35-plex TMTpro-MS to analyze CSF and plasma from healthy controls (n= 28, n= 31) and sporadic ALS (n= 38, n= 40) from the Target ALS Global Natural History Study. Measured CSF and plasma proteins were also benchmarked to Simoa NfL immunoassay measures and correlated to ALS functional decline. This initial cross-sectional proteomic study highlights the potential of this resource as a potent platform for ALS biomarker discovery.

## Methods & Cohort

- **Cohort & Protocol**: Cerebrospinal fluid (CSF) and plasma were collected across 7 academic clinical sites from healthy controls (CSF: n=28; plasma: n=31) and sporadic ALS (sALS) patients (CSF: n=38; plasma: n=40) enrolled in the Target ALS Global Natural History Study. All participant biosamples are linked to clinical data including participant demographics, clinical data (i.e. ALSFRS-R, respiratory measures), and genetics.
- **35-plex TMTpro-MS**: Samples underwent high-abundance protein depletion (High Select Top14, Thermo Scientific, followed by tryptic digestion and TMTpro 35-plex labeling (Thermo Scientific). Multiplexed sets were fractionated prior to LC-MS/MS analysis on an Orbitrap (Thermo Scientific) mass spectrometer.
- **Simoa NfL Immunoassay**: CSF and plasma NfL concentrations were measured using the NF-Light v2 Advantage kit on a Simoa HD-X analyzer (Quanterix). The assay was performed as per the manufacturer's protocol.
- **Statistics**: Pairwise comparisons between sALS and controls utilized Welch's t-test with Benjamini-Hochberg multiple testing correction to identify significant differential expression (adjusted p-value < 0.05).

## Fig 1. CSF 35-Plex TMTpro-MS robustly detects established and novel ALS biomarkers

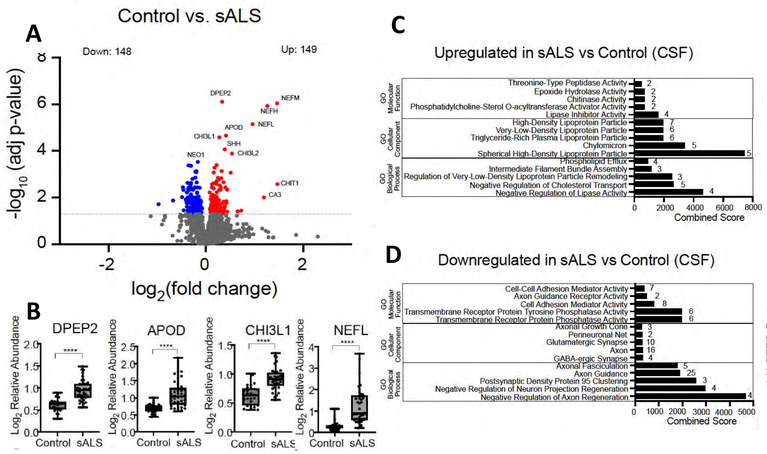


**Fig 1. A)** Volcano plot of CSF differentially expressed proteins (DEPs) between sALS (n=38) and healthy controls (n=28) (adj p < 0.05). **B)** Box plots displaying log2 relative abundances of select significant DEPs including dipeptidase 2 (DPEP2), Apolipoprotein D (APOD), chitinase 3-like protein 1 (CHI3L1), and neurofilament light (NEFL). Gene Ontology (GO) enrichment analysis for **C)** up-regulated proteins and **D)** down-regulated proteins.

## Fig 2. Plasma 35-Plex TMTpro-MS identifies muscle-enriched and inflammatory markers

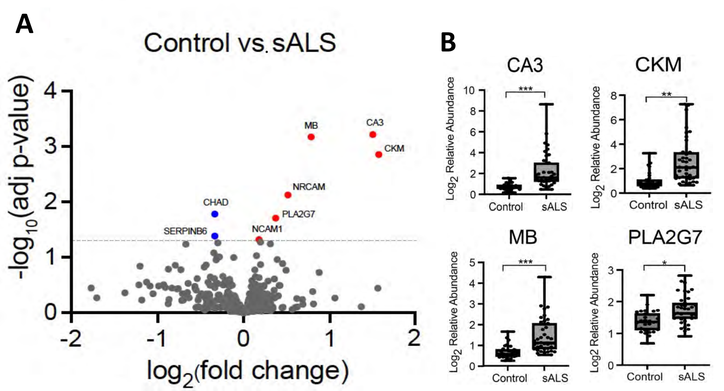


**Fig 2. A)** Volcano plot of plasma DEPs comparing sALS (n=40) to controls (n=31). **B)** Box plots displaying log2 relative abundances of the top significantly increased proteins, carbonic anhydrase 3 (CA3), creatine kinase muscle (CKM), myoglobin (MB), phospholipase A2 group 7 (PLA2G7).

## Fig 3. Correlation of ALS biofluid proteome to ALS functional decline

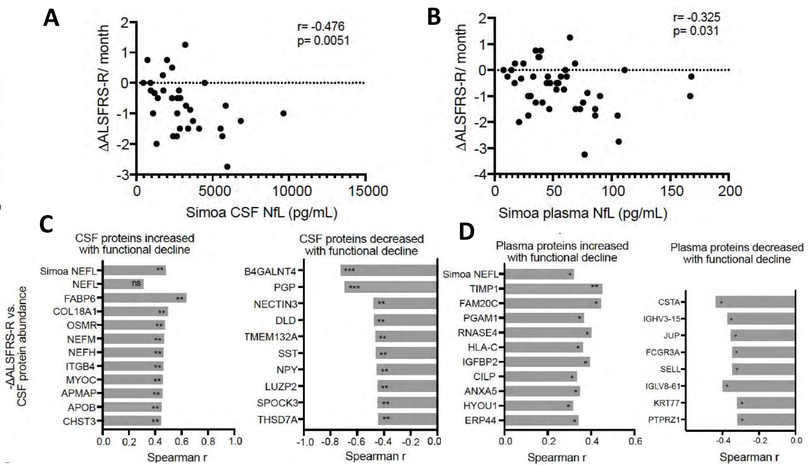


**Fig 3.** Correlation of Simoa NfL measures to clinical rate of functional decline (ΔALSFRS-R/month). In **A)** CSF and **B)** plasma **B)** Bar charts ranking the top up- and down-regulated 35-plex TMTpro-MS proteins by their Spearman correlation to functional decline in **C)** CSF and **D)** plasma, revealing putative candidates with comparable or superior prognostic value to Simoa NfL.

## Conclusions

- 35-plex TMTpro-MS provides deep, unbiased coverage of the CSF and plasma ALS proteome.
- In CSF, differentially expressed proteins in ALS included known biomarkers (i.e. NEFL, NEFM, NEFH, CHIT1, CHI3L) as well as novel targets
- In plasma, 35-plex TMTpro-MS captured systemic muscle and inflammatory alterations.
- CSF and plasma DEPs as well as putative biomarkers of functional decline will require further longitudinal validation in larger clinical cohorts.

## Acknowledgements

We thank the participants, their families, and caregivers for their invaluable contributions to the study. We gratefully acknowledge Target ALS for their support.

## References

1 Chia R, Moaddel R, Kwan JY, et al. A plasma proteomics-based candidate biomarker panel predictive of amyotrophic lateral sclerosis. Nat Med. Oct 2025;31(10):3440-3450. doi:10.1038/s41591-025-03890-6

2 Dergai O, Wuu J, Kozlczak-Holbro M, et al. Skeletal Muscle Biomarkers of Amyotrophic Lateral Sclerosis: A Large-Scale, Multi-Cohort Proteomic Study. Ann Neurol. 2026;99(2):393-407. doi:10.1002/ana.78046

3 Khalil M, Teunissen CE, Lehmann S, et al. Neurofilaments as biomarkers in neurological disorders - towards clinical application. Nat Rev Neurol. May 2024;20(5):269-287. doi:10.1038/s41582-024-00955-x

4 Zhan Z, Liang H, Zhao Z, et al. The Trim32-DPEP2 axis is an inflammatory switch in macrophages during intestinal inflammation. Cell Death Differ. Jul 2025;32(7):1336-1352. doi:10.1038/s41418-025-01468-w

5 Candels LS, Becker S, Trautwein C. PLA2G7: a new player in shaping energy metabolism and lifespan. Signal Transduct Target Ther. Jun 17 2022;7(1):195. doi:10.1038/s41392-022-01052-5

# ACE-2223, a novel oral small molecule, treats both gain- and loss-of-function TDP-43 pathology, extends survival and decreases NfL in mice

**Vidhu Mathur**, Marcela Kokes, Shruti Arya, Devi Korumilli, Vanessa Seawright, Lewis Whitehead, Katie Planey
Acelot Inc., South San Francisco, CA, USA

## Abstract

Background: RNA binding protein TARDBP (TDP-43) pathology is in > 97% of non-genetically modified Amyotrophic Lateral Sclerosis (ALS) patients. TDP-43 dysfunction involves both loss of nuclear TDP-43 and gain of TDP-43 cytoplasmic aggregates; targeting this dysfunction may slow the progression of ALS. ACE-2223, a novel orally bioavailable small molecule that directly targets aggregated TDP-43 and restores the functional form of TDP-43.
Methods: ACE-2223 binding and activity on TDP-43 aggregates was confirmed using multiple biophysical and biochemical methods. Cell based experiments used reporter cell lines and iPSC-derived neurons. In vivo activity of ACE-2223 was tested in iTDP43$^{A315T}$ and rNLS8 (ΔNLS-hTDP43) mice. IND-enabling studies including 28-day GLP toxicology studies are complete and chronic toxicology is ongoing.
Results: ACE-2223 directly binds and disrupts recombinant and human ALS brain derived TDP-43 aggregates. In cellular models of TDP-43 pathology, ACE-2223 reduces insoluble cytoplasmic TDP-43, increases nuclear TDP-43 and rescues TDP-43 dependent mis-splicing in mRNAs including STMN2 and UNC13A. In the iTDP43$^{A315T}$ mouse model, ACE-2223 treatment showed high brain penetrance, reduced TDP-43 pathology and rescued neuroinflammation and behavioral phenotypes. In rNLS8 mouse model, ACE-2223 significantly improved survival and reduced plasma Nf-L. A comparison of the levels of aggregated TDP-43 in ALS human motor cortices and rNLS8 mouse brains along with human dose modeling projects that ACE-2223 can be administered at efficacious doses in humans.
Summary: ACE-2223 potently disrupts TDP-43 aggregates in ALS *in vitro* and *in vivo* models resulting in functional improvements such as decreased cryptic exons, decreased Nf-L and improved survival.
Healthy volunteer clinical trial to test safety and tolerability of ACE-2223 has initiated. ALS clinical trials are planned for 2027.

## ACE-2223 Mechanism of action

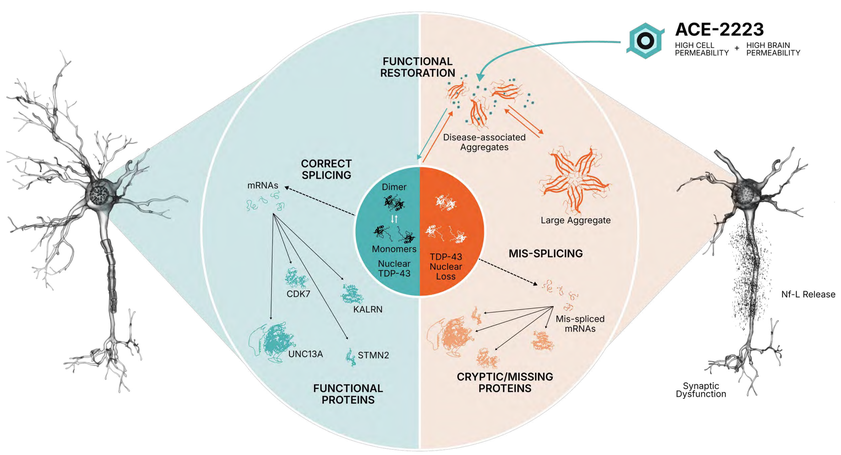


Illustration showing that TDP-43 functions in the nucleus in healthy neurons, while in ALS, TDP-43 is forms cytoplasmic inclusions and loses function. ACE-2223 directly disrupts TDP-43 aggregates and restores TDP-43 localization and function thereby rescuing neuronal health and ALS associated disease phenotypes.

## ACE-2223 prevents de novo formation and disrupts pre-formed TDP-43 aggregates

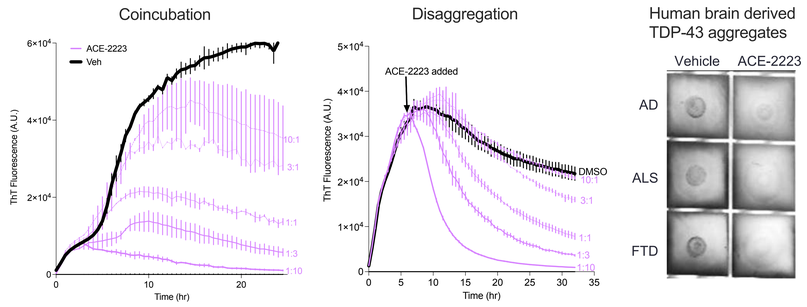


**ACE-2223 directly inhibits TDP-43 aggregation.** Recombinant TDP-43 peptide aggregation was monitored in a Thioflavin T (ThT) dye binding kinetic assay. ACE-2223 dose dependently prevented TDP-43 aggregate formation when co-incubated with monomeric protein (left) and disrupted preformed TDP-43 steady state aggregates (middle). Stoichiometric ratios of TDP-43:ACE-2223 are shown.
ACE-2223 also dissociated TDP-43 aggregates derived from human ALS, FTD and AD post-mortem brain tissues measured using TDP-43 specific antibodies on a dot blot (right) .

## ACE-2223 decreases cytoplasmic TDP-43 aggregates

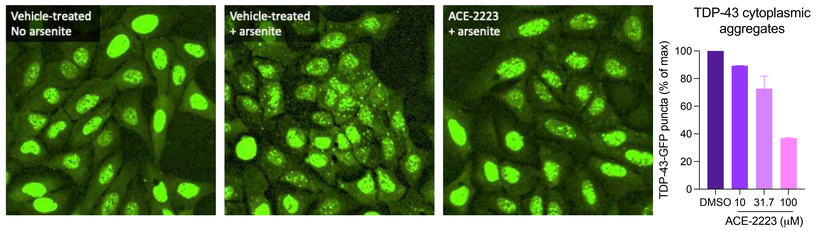


**ACE-2223 reduces cytoplasmic aggregated TDP-43 in an oxidative stress model.** U2OS reporter cell model overexpressing TDP-43-GFP were induced to form cytoplasmic puncta using 250uM sodium arsenite in the presence of ACE-2223. Representative images and quantification shown.

## ACE-2223 restores nuclear TDP-43

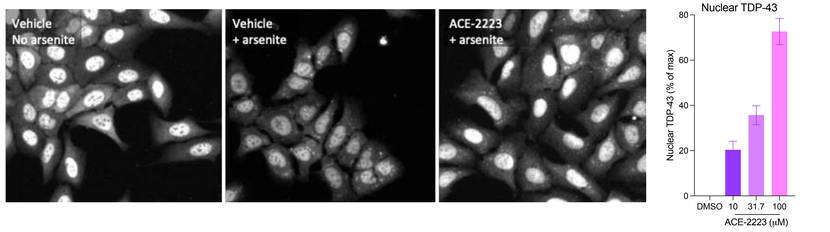


**ACE-2223 restores nuclear TDP-43 in an oxidative stress model.** U2OS cellular model for nuclear TDP-43 rescue shows endogenous TDP-43 nuclear loss upon 250uM sodium arsenite treatment. Representative images and quantification showing ACE-2223 rescues nuclear TDP-43.

## ACE-2223 rescues cryptic exons

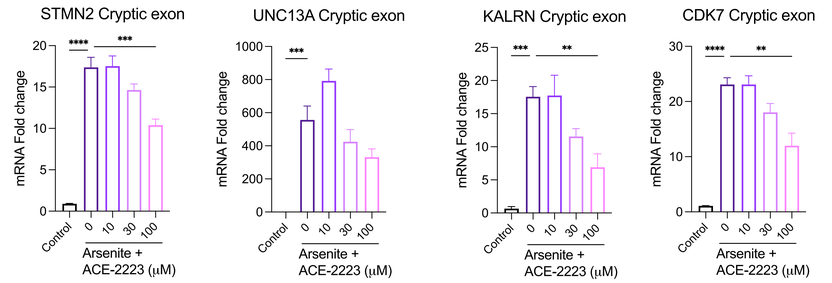


**ACE-2223 rescues splicing function in iPSC-neurons.** ACE-2223 rescues TDP-43 dysfunction dependent cryptic exons in indicated mRNAs in iPSC-derived motor neurons treated with sodium arsenite (250μM for 2h). Assays shown use sodium arsenite, an aggressive TDP-43 aggregation model, and thus require high dosing.

## ACE-2223 rescues pathology in iTDP43$^{A315T}$ mice

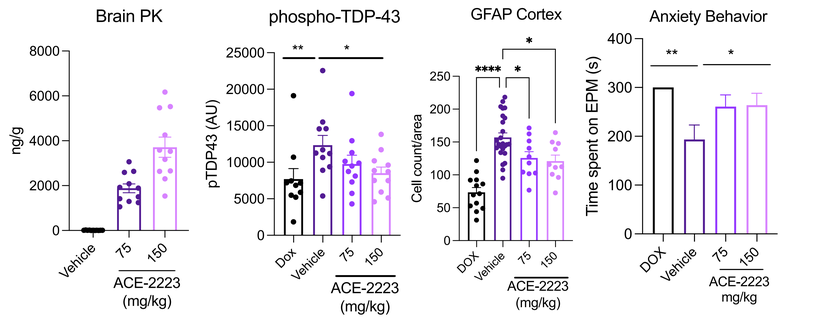


**ACE-2223 rescues disease phenotypes in iTDP43$^{A315T}$ mice.** ACE-2223 was dosed once daily per orally from 4 to 12 weeks of age. ACE-2223 showed high dose dependent drug levels in the mice brain tissue (PK), reduced disease associated TDP-43: insoluble, phosphorylated (shown here), ubiquitinated and cytoplasmic TDP-43 in mouse brain tissue, rescued astrogliosis measured by GFAP immunostaining in mouse brain tissue and rescued motor and anxiety behavior (shown here) phenotypes.

## ACE-2223 rescues NfL and survival in rNLS8 mice

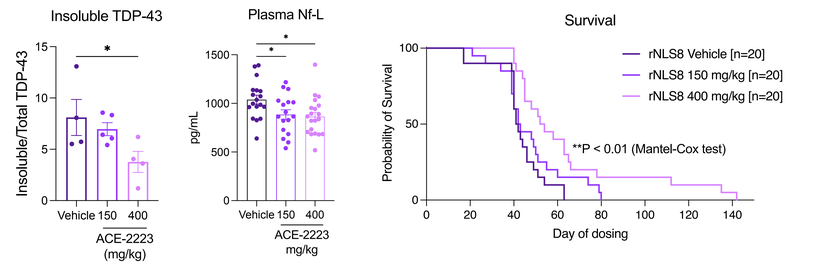


**ACE-2223 rescues disease phenotypes in rNLS8 DOX OFF mice.** ACE-2223 was dosed once a day per orally starting at the time of DOX OFF. ACE-2223 reduced insoluble TDP-43 in the brains of rNLS8 mice and significantly reduced plasma NfL after 4 weeks of dosing. ACE-2223 also significantly improved survival in rNLS8 mice.
Statistics for all figures: Mean±SEM are shown. P<0.05*, P<0.01**, P<0.001***, P<0.0001**** One-way ANOVA followed by Kruskal-Wallis test.

# Blocking RAN translation without altering repeat RNAs rescues *C9ORF72*-related ALS and FTD phenotypes


Xin Jiang[1,2], Laure Schaeffer[3], Divya Patni[1], Tommaso Russo[1,4], Chao-Zong Lee[1], Corey Aguilar[1,2], Christine Marques[1], Karen Jansen-West[5], Marian Hruska-Plochan[6], Ananya Ray-Soni[1,2], Su Min Lim[1,2], Aaron Held[1], Mei Yue[5], Paula Otero[5], Sandeep Aryal[1,2], Hortense D.A.M. Beaussant[1], Himanish Basu[7], Hiro Takakuwa[8], Lillian M. Daughrity[5], Nandini Ramesh[1,2], Paulo Da Costa[3], Ana Rita A. A. Quadros[1,2], Matthew Nolan[1,2], Charles Jourdan F. Reyes[1,2], Hayden Wheeler[1], Laura C. Moran[1], Grant Griesman[1], Benjamin Wymann[1], Bianca A. Trombetta[1], Emma Sofia Lopez-De-Sillanes[1], Michael Canori[1,2], Gopinath Krishnan[9], Yasmim Vieira Souza Da Silva[1], Gilbert Eriani[3], Mark W. Albers[1], Steven E. Arnold[1], Yuyu Song[1,10], Ankur Jain[8,11], Isaac M. Chiu[7], Brian J. Wainger[1,2], Yong-Jie Zhang[5], Fen-Biao Gao[9], Magdalini Polymenidou[6], Leonard Petrucelli[5], Franck Martin[3*], Clotide Lagier-Tourenne[1,2*]

[1] Department of Neurology, Massachusetts General Hospital, Harvard Medical School, Boston, MA, USA. [2] Broad Institute of Harvard University and MIT, Cambridge, MA, USA. [3] Architecture et Réactivité de l'ARN, UPR 9002, Université de Strasbourg, CNRS, Strasbourg, France. [4] Neurology Unit and Experimental Neuropathology Unit, Institute of Experimental Neurology, Division of Neuroscience, IRCCS San Raffaele Scientific Institute, Milan, Italy. [5] Department of Neuroscience, Mayo Clinic, Jacksonville, FL, USA. [6] Department of Quantitative Biomedicine, University of Zurich, Zurich, Switzerland. [7] Department of Immunology, Harvard Medical School, Boston, MA, USA. [8] Whitehead Institute for Biomedical Research, Cambridge, MA, USA. [9] Frontotemporal Dementia Research Center, RNA Therapeutics Institute, University of Massachusetts Chan Medical School, Worcester, MA, USA. [10] Marine Biological Laboratory, Woods Hole, MA, USA. [11] Department of Biology, Massachusetts Institute of Technology, Cambridge, MA, USA. *Corresponding authors



## Abstract

**Background**: Expansion of $G_4C_2$ repeats in a non-coding region of the *C9ORF72* gene is the most common inherited cause of amyotrophic lateral sclerosis (ALS) and frontotemporal dementia (FTD). The expansion produces sense $G_4C_2$ and antisense $G_4C_2$ repeat-containing RNA foci and five dipeptide repeat proteins (DPRs) through repeat-associated non-AUG (RAN) translation. Our previous work showed that translation of $G_4C_2$ transcripts at the *C9ORF72* locus initiates at a near-cognate CUG codon upstream of the repeats. Importantly, mutating this CUG codon suppresses translation in all three reading frames without affecting RNA foci formation, providing a unique tool to dissect the relative contributions of repeat RNA and DPR toxicity to neurodegeneration.

**Methods**: To investigate the effect of mutating the CUG start codon in vivo, we performed intracerebroventricular injections of adeno-associated virus expressing G4C2 repeats with either the native CUG or a mutated CCG start codon in mice. We generated both shorter (66 repeats) and longer (150 repeats) repeat models to examine whether repeat length influences the impact of CUG-dependent translation. To assess DPR versus repeat RNA toxicity in a more physiological context, we precisely edited the CUG codon in *C9ORF72* patient-derived iPSC lines and analyzed phenotypes in iPSC-derived neurons.

**Results**: In both AAV mouse models, the CUG to CCG mutation markedly reduced RAN translation and suppressed accumulation of DPR proteins from all three reading frames. Blocking RAN translation without altering *C9ORF72* transcripts or RNA foci rescued ALS/FTD-related hyperactivity and motor deficits in mice. It also reduced pTDP-43 aggregation, prevented motor neuron loss, and suppressed activation of the STING–pTBK1 pathway. In addition, the mutation alleviated neuroinflammation and restored plasma neurofilament light levels. Base editing of the CUG codon in patient iPSC-derived neurons similarly reduced DPR accumulation and improved gene expression profiles, neuronal survival, neurite growth, protein localization, and STING pathway activation.

**Summary**: These findings demonstrate a central role for DPRs in *C9ORF72*-mediated neurodegeneration and highlight the therapeutic potential of targeting DPR production rather than repeat RNA.


## Methods and workflow

### (1) Expressing $G_4C_2$ repeats with CUG or CCG in a mouse model


### (2) Mutating CUG to CCG in C9ORF72 iPSC by CRISPR base editing

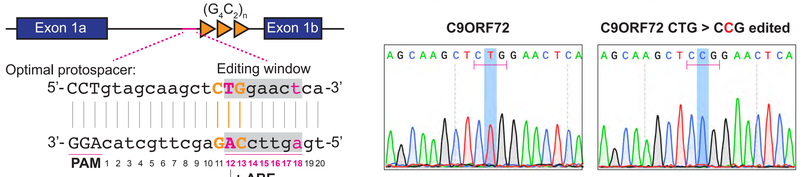


## CUG>CCG mutation blocks sense DPR translation in AAV-C9ORF72-$(G_4C_2)_{66}$ mice

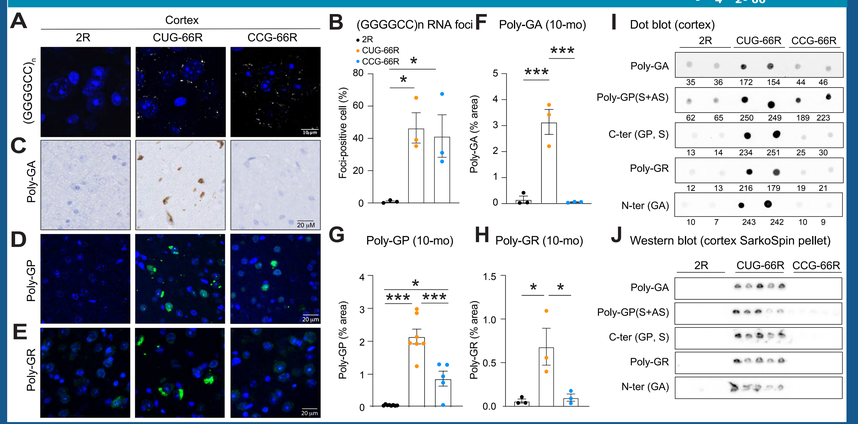


(**A, B**) Fluoresence *in situ* hybridization (FISH) with probe targeting $G_4C_2$ repeat-containing RNAs in the mouse brain. The percentage of cell which positive for foci were quantified, n=3 mice/genotype. (**C-H**) Immunostaining with antibody against poly-GA, poly-GP, and poly-GR in the brain from 10-month-old mice. The percentage area covering by DPR-positive pixel were quantified, n=3-7 mice/genotype. (**I**) Dot blot and Western blot (**J**) showing the DPR expressions in total cortex lysates (I) or SarkoSpin pellet fractionation of cortex tissue (J) from 15-month-old mice.

## CUG>CCG mutation rescues behavior deficits of AAV-C9ORF72-$(G_4C_2)_{66}$ mice

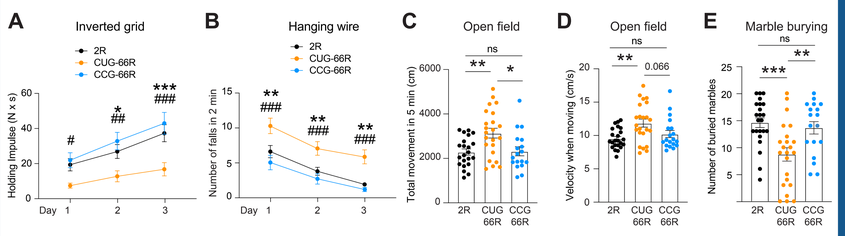


(**A**) Inverted grid test performed in 9-month-old mice expressing $(G_4C_2)_{66}$ with either a CUG or mutated CCG codon upstream of the repeat. Holding impulse = body weight (g) x 0.00980665 (N/g) x hanging time (s), n = 18-23 mice per genotype, both males and females. (**B**) Hanging wire test determined the number of falls within 2 min in 9-month-old mice. N = 14-20 mice per genotype, mean ± SEM, *: differences between 2R and CUG-66R; #: differences between CUG-66R and CCG-66R. (**C, D**) Open field test in 8-month-old mice to determine the total movement (C) and mobility time (D) during the first 5 min of recording. (**E**) Marble buryingassay was performed in 8-month-old mice. The number of buried marbles was counted after placing the mouse in the cage for 5 min.N = 20 mice per genotype, mean ± SEM.

## CUG>CCG mutation rescues pathological deficits of AAV-C9ORF72-$(G_4C_2)_{66}$ mice

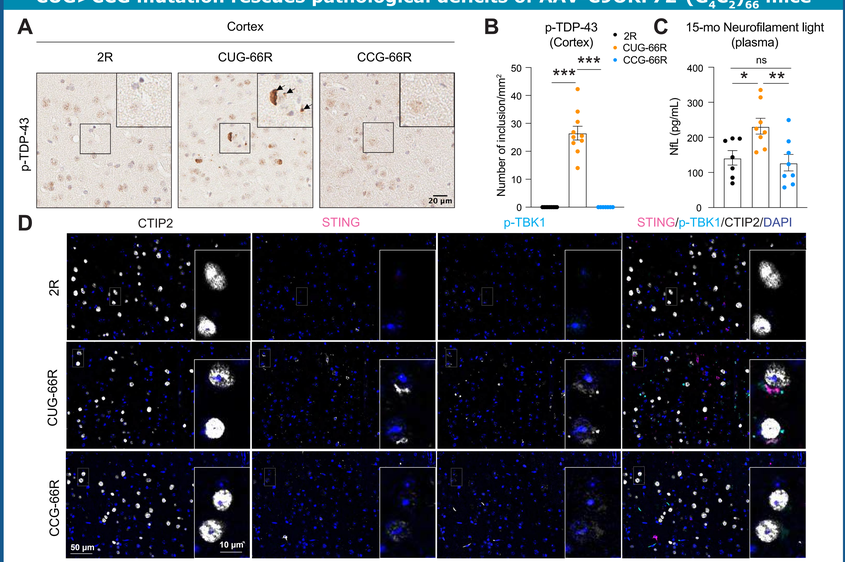


(**A, B**) Immunohistochemistry staining with phosphorylated TDP-43 (p-TDP-43) antibody in cortex of 15-month-old mice. The arrowheads in the insert point to p-TDP-43 aggregates. The number of inclusions per mm2 was quantified in the whole cortex. N=8 mice per genotype, mean ± SEM. (**C**) Neurofilament light (NfL) concentration in plasma of 15-month-old mice. N= 6-8 mice per genotype, mean ± SEM. (**D-H**) Immunofluorescence staining of the layer V motor cortex in 15-month-old mice with antibodies against CTIP2, STING, and p-TBK1 (D). The number of CTIP2-positive neurons in layer V of the motor cortex (E), the percentage of CTIP2-positive cells with accumulation of STING (F), p-TBK1 (G), or both STING and p-TBK1 (H) were determined. N=10 mice per genotype, mean ± SEM. (**I-K**) Immunohistochemistry staining with antibodies against the astrocytes marker GFAP and activated phagocytic microglia marker CD68 in cortex of 15-month-old mice expressing $(G_4C_2)_{66}$ with either a CUG or mutated CCG codon upstream of the repeat. The number of GFAP-positive cells per mm2 (J) and the percentage of area covered by CD68-positive pixel (K) were quantified. N=8 mice per genotype, mean ± SEM. (**L**) Immunoblot showed the level of Polyubiquitin (K48) in the SarkoSpin pellet fraction from the cortex of 15-month-old mice


**FUNDINGS** 1. Development Grant 21 from Muscular Dystrophy Association **2.** Milton Safenowitz postdoctoral fellowship from ALS Association **3.** Sean M. Healey & AMG Center for ALS **4.** TargetALS **5.** NIH **6.** Chan Zuckerberg Initiative


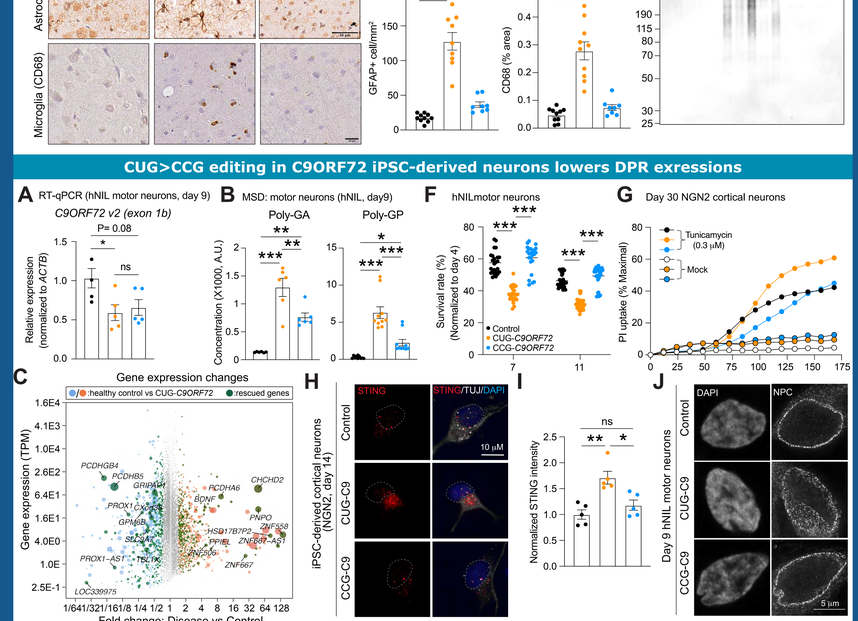


## CUG>CCG editing in C9ORF72 iPSC-derived neurons lowers DPR exressions

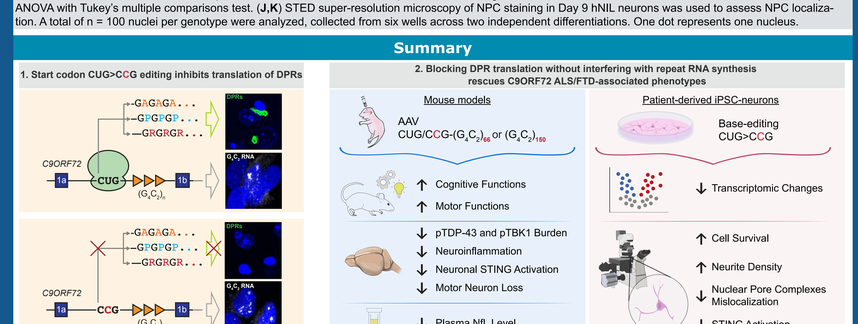


(**A**) RT-qPCR showing reduced expression of the C9ORF72 transcript variant 2 in both CUG and CCG edited C9ORF72 iPSC-derived motor neurons. N = 5; mean ± SEM. (**B**) DPR levels in the Day-9 hNIL neurons were assessed by immunoassay. N=3 independent differentiation, each dot represents one technical replicate from immunoassay (**C**) Volcano plot displaying differentially expressed genes in day 9 hNIL motor neurons. Genes with significant changes in mRNA levels between control and CUG-C9ORF72 are represented by blue or red dots. Dot size is inversely proportional to the statistical significance. Green dots represent genes rescued in the CCG-C9ORF72. The labeled genes are the top 10 rescued genes ranked by p.adjust on the up- or down-regulated side. N=5 biological replicates/genotype from 3 independent differentiation experiments. (**D**) Pie chart illustrating the proportion of up- and down-regulated genes between control and CUG-C9ORF72, and the proportion of genes rescued in CCG-C9ORF72. (**E**) Gene Ontology (GO) Molecular Function terms in genes which differentially expressed genes between control and CUG-C9ORF72 and rescued in CCG-C9ORF72 (ranked by FDR). (**F**) The number of alive hNIL neurons was counted on day 7 and day 11. Numbers on each day normalized to day 4 as the survival rate. N=4 independent differentiation, each dot represents the value from one well. (**G**) NGN2 neurons were incubated in propidium iodide (PI)-containing medium and treated with 0.3 μM tunicamycin. (**H,I**) The intensity of STING signal in TUJ1-positive neurons was quantified, and the data was normalized to the control line. pendent differentiations, each dot represents the averaged value from 15 to 25 fields of view/well. Mean ± SEM, one-way ANOVA with Tukey's multiple comparisons test. (**J,K**) STED super-resolution microscopy of NPC staining in Day 9 hNIL neurons was used to assess NPC localization. A total of n = 100 nuclei per genotype were analyzed, collected from six wells across two independent differentiations. One dot represents one nucleus.

## Summary